AMPTIAC

MECHANISM AND KINETICS OF CORROSION OF SELECTED IRON AND COBALT ALLOYS IN REFLUXING MERCURY

by Louis Rosenblum, Coulson Scheuermann,
Charles A. Barrett, and Warren H. Lowdermilk

Lewis Research Center
Cleveland, Ohio

20060516253

NASA TN D-4450

MECHANISM AND KINETICS OF CORROSION OF SELECTED IRON AND

COBALT ALLOYS IN REFLUXING MERCURY

By Louis Rosenblum, Coulson Scheuermann, Charles A. Barrett,
and Warren H. Lowdermilk

Lewis Research Center
Cleveland, Ohio

NATIONAL AERONAUTICS AND SPACE ADMINISTRATION

MECHANISM AND KINETICS OF CORROSION OF SELECTED IRON AND

COBALT ALLOYS IN REFLUXING MERCURY

by Louis Rosenblum, Coulson Scheuermann, Charles A. Barrett,
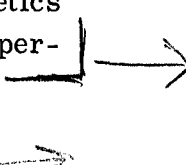and Warren H. Lowdermilk

Lewis Research Center

SUMMARY

Five alloys of engineering interest, the cobalt-base HS-25 and H-8187 and the iron-base SICROMO-9M, AM-350, and AM-355, were corrosion tested in boiling mercury in the temperature range of 1000° to 1300° F (811° to 977° K) for times as long as 5000 hours. Metallographic, chemical, and physical analyses were used to determine the extent and the nature of the corrosion.

Corrosion mechanism and reaction kinetics were inferred through a comparison of experimental and theoretical kinetic constants. The experimental kinetic constants (i.e., the time-law constant b_r and the activation energy ΔH_r) were obtained from the test data by multiple regression analysis. The theoretical kinetic constants b_i and ΔH_i for each of i steps of proposed corrosion models were obtained from transport theory relations and the pertinent boundary conditions.

Changes of mechanism during the progress of corrosion were indicated for all the alloys tested except the AM-350 and AM-355 alloys. The shifts from one corrosion regime to another were associated with changes in the nature and length of the corrosion-affected zone. Three corrosion regimes were characterized, linear I, parabolic, and linear II. The probable rate-determining step in the two linear rate regimes is boundary-layer diffusion. The probable rate-determining step in the parabolic rate regime is liquid diffusion.

INTRODUCTION

The present interest in space power systems that employ mercury as the thermo-dynamic working fluid at temperatures in the range of 1000° to 1200° F (811° to 922° K) (refs. 1 and 2) has prompted the need for an understanding of the mechanism and kinetics of mercury corrosion. Such knowledge could be an invaluable guide in establishing oper-

ational limits, extrapolating performance, and translating small-scale test results to larger system applications.

According to the prevailing concepts of reaction mechanisms, a reaction such as the corrosion of a solid material by mercury occurs as a sequence of steps. The combined effect of these steps determines the net rate of the reaction. However, if, as is common, one step is significantly slower than the others, the rate of the entire reaction is governed by the slowest step. In cases where the slow step involves a diffusion process (e.g., volume diffusion in a solid), the reaction is termed diffusion controlled and is governed by the laws of diffusion kinetics. Alternately, if a boundary-region process (e.g., solution) constitutes the slow step, the rate of the overall reaction is determined by the kinetics of this process.

The kinetics of each step of a corrosion mass-transport reaction can be expressed by the empirical relation

$$w_i = k_i t^{b_i} \tag{1}$$

where w_i is a measure of the mass transported, b_i is the time-law constant for the ith step, and t is time. The quantity k_i is known as the specific rate constant for the ith step and is a function of temperature only; that is,

$$k_i = a_i \exp\left(-\frac{\Delta H_i}{RT}\right) \tag{2}$$

where a_i is a constant, R is the gas constant, T is absolute temperature, and ΔH_i is the "energy of activation" of the ith step.

Therefore, when a corrosion reaction is governed by one controlling step, the mass transport and the specific rate constant for the entire reaction will be equal to, respectively, the mass transport w_s and the specific rate constant k_s of the rate-controlling step. This relation, then, forms a basis for determining the mechanism and kinetics of corrosion.

Only two mechanism studies of high-temperature dynamic mercury corrosion have been reported (refs. 3 and 4). In each study the same data were used, namely, the data for the corrosion of low-carbon steel in mercury over the temperature range of 900° to 1200° F (755° to 922° K) presented in reference 5. Nevertheless, each study reached a different conclusion as to the mechanism of attack. The basic approach followed can be summarized as follows:

(1) An assumption was made of the rate-controlling step.

(2) A heat-transfer - mass-transfer analog equation was derived for k_s.

2

(3) Estimates were made of the mass-transfer coefficients and empirical constants of the heat-transfer - mass-transfer analog equation and a solution was obtained for k_s.

(4) The experimentally observed corrosion rate was compared with k_s for agreement.

(5) The activation energy derived from the experimental data was compared for agreement with the activation energy estimated to be associated with the assumed rate-controlling step.

In the first study (ref. 3), liquid-boundary-layer diffusion was assumed to be the rate-controlling process. Order-of-magnitude agreement was obtained between the rate predicted by the derived heat-transfer - mass-transfer analog equation and the observed corrosion rate. The order-of-magnitude agreement between observation and theory was considered to justify the general validity of the premises made.

A second study (ref. 4) used the same data and mass-transfer equation as the first study. It was concluded therein that the difference between the estimated and experimental activation energies and the disparity between the observed and theoretical corrosion rate suggested that a process other than diffusion-control solution attack (probably intergranular attack) is the controlling factor in the corrosion of steel by mercury.

For completeness, corroboration of a corrosion mechanism by this approach requires the formulation of a number of corrosion-rate equations equal to the total number of possible rate-determining steps. Concomitantly, values of the pertinent material-transport coefficients and empirical constants are required to solve each equation. In many instances, these values have not been determined or are not known accurately.

In the present study, a somewhat different approach was used. No assumption of a rate-controlling step was made. Rather, rate and rate-controlling step were inferred from a comparison of experimental and theoretical kinetic constants. The major problem of this approach is the paucity of available data needed in the estimate of activation energy for several pertinent processes. In brief, the approach was as follows:

(1) Values of the experimental kinetic constants b_r and ΔH_r were obtained from a multiple linear regression fit of the corrosion data to the estimating equation

$$\log p_r = a_r + b_r \log t + \frac{\Delta H_r}{2.303 \, RT} \tag{3}$$

where p_r is observed maximum corrosion penetration or wall recession (assumed to be proportional to w_r), t is test time, T is test temperature, and a_r is a constant. Equation (3) was derived by the elimination of k between equations (1) and (2) (where the subscript r replaces i).

(2) A corrosion model was constructed consistent with the general nature of the observed corrosion attack. For each step of the corrosion model, an equation was derived

(from considerations of transport theory and the relevant boundary conditions) in the form of equation (1), which yielded b_i directly.

(3) Values of ΔH_i were obtained from the relation

$$\Delta H_i = \frac{R \, d(\ln k_i)}{d\left(\dfrac{1}{T}\right)} \tag{4}$$

which is the differential form of equation (2).

(4) The theoretical kinetic constants ΔH_i and the b_i for each step in the proposed corrosion mechanism were compared with ΔH_r and b_r, respectively. Agreement of the theoretical kinetic constants for the ith step with the respective experimental kinetic constants was taken to infer that the ith step is rate determining.

The method of data analysis employed in this approach provides a ready opportunity to test for the possibility of mechanism changes during the process of corrosion. Such changes may be expected, inasmuch as corrosion induces physical changes in the test material which can lead to changes in the material-transport path and, thereby, in the rate-controlling step. This process is analogous to certain oxidation reactions where changes in oxidation kinetics accompany changes in the thickness or adherence of oxide layers (ref. 6). The possibility of mechanism changes during the course of corrosion was explored. First, the data for each test material were grouped on the basis of the physical appearance of the corroded area. Second, a multiple linear regression fit of the grouped data to equation (3) was made. Third, a statistical goodness-of-fit comparison was made between the grouped and nongrouped data.

For the experimental part of this study, 108 reflux capsule tests were performed on five materials of engineering interest, AM-350, AM-355, SICROMO-9M, HS-25, and H-8187. The test temperature range was 1000° to 1300° F (811° to 977° K) and test times were as long as 5000 hours. Metallographic analyses were performed on all test specimens to determine corrosion penetration. In addition, chemical and physical analyses were performed on selected specimens to determine the composition of the corrosion zones, the corrosion deposits, and the bulk alloys. (The authors express their appreciation to Dr. Leo F. Epstein of General Electric Vallecitos Laboratory and Dr. Malcolm Parkman of Varian Associates, Palo Alto, California for helpful review and for pointing out an error in activation-energy estimation in the original manuscript.)

4

EXPERIMENT

Procedure

The effect of mercury corrosion on HS-25, H-8187, SICROMO-9M, AM-350, and AM-355 was determined by means of reflux capsule tests wherein the capsule wall served as the test specimen. Table I lists the composition of the test alloys and table II lists the forms in which they were received, their prior history, and their sources.

TABLE I. - COMPOSITION OF TEST ALLOYS

Alloy	Ni	Co	Fe	Cr	Mn	Mo	W	Other
	wt. %							
HS-25	9.9	51.1	2.5	19.8	1.2	---	15.5	---------
H-8187	1.2	64.6	1.1	20.6	.6	0.1	11.8	---------
SICROMO-9M	---	----	90.3	8.6	.5	.6	----	---------
AM-350	4.1	----	75.1	16.6	1.1	2.9	----	0.2 (N+C)
AM-355	4.3	----	76.2	15.5	1.0	2.8	----	.2 (N+C)

TABLE II. - FORM, HISTORY, AND SOURCE OF TEST ALLOYS

| Alloy	Form	History	Source
HS-25	1/2-in. (1.27-cm) round stock, centerless ground	Solution treated at 2250° F (1505° K)	Haynes Stellite Co.
H-8187	2-in. (5.08-cm) hot-worked square	Solution treated at 2250° F (1505° K)	Haynes Stellite Co.
SICROMO-9M	1-in. (2.54-cm) round stock	Annealed at 1650° F (1171° K), cooled 50° F (28° K) per hour	Timken Roller Bearing Co.
AM-350	9/16-in. (1.43-cm) rod, centerless ground	Annealed at 1425° F (1047° K), air cooled	Allegheny-Ludlum Steel Corp.
AM-355	9/16-in. (1.43-cm) rod, centerless ground	Annealed at 1025° F (825° K), air cooled	Allegheny-Ludlum Steel Corp.
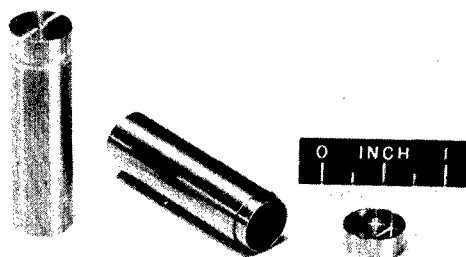
C-58680

Figure 1. - Reflux capsule.

Capsule preparation. - Capsules (fig. 1) were machined from the as-received stock to the nominal dimensions of 1/2-inch (1.27-cm) outside diameter, $1\frac{3}{4}$ inches (4.45 cm) in length and 0.040-inch (0.102-cm) wall thickness. The inner surfaces were lapped to a mirror-like finish. The capsules were then degreased and chemically cleaned.

Next, the capsules were filled to approximately one-third their volume with film-free, triple-distilled mercury and sealed by electron-beam welding in a vacuum of about 10^{-5} torr (10^{-3} N/m^2). During the welding process, which took less than 8 seconds, the capsules were held in a water-cooled jacket to prevent vaporization of the mercury. Heat treatment of the capsule as a result of the weld was confined to the vicinity of the weld. The sealed capsules were inspected radiographically to check the mercury level and the degree of wetting of the capsule wall.

Capsule testing. - The capsules were tested in argon. Heating of the capsules was accomplished by means of individual capsule furnaces which supplied heat to the lower two-thirds of the capsule. The furnaces consisted of a Nichrome wire winding on a magnesium silicate core surrounded on the sides and bottom with 0.375 inch (0.952 cm) of magnesium silicate. The tops of the capsules were exposed so that heat was lost to the environment by natural convection and radiation.

Test beds of 10 furnaces were employed (fig. 2). Each furnace was individually controlled to within $\pm 10°$ F ($\pm 5.5°$ K) of a preset temperature by its own powerstat. Chromel-Alumel thermocouples spot welded to the top and bottom capsule surface were

6
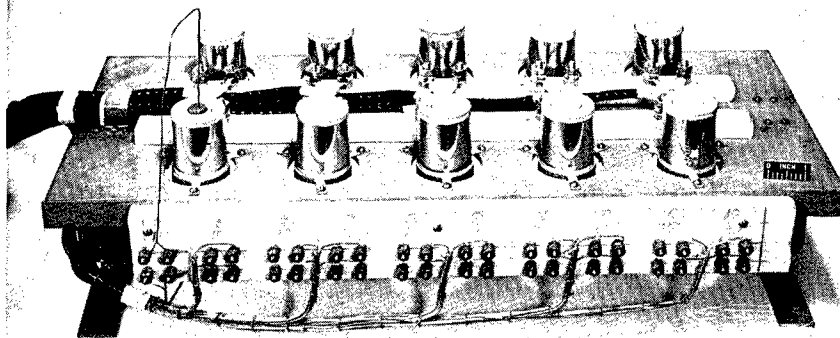
C-55896

Figure 2. – Test bed used for reflux capsule testing.

used to measure temperature. The thermocouple output was continuously recorded on a multipoint strip-chart recorder.

Tests were conducted at 1000°, 1100°, 1150°, 1200°, 1250°, and 1300° F (811°, 866°, 894°, 922°, 950°, and 977° K); test times were as long as 5000 hours. The temperature indicated by the bottom thermocouple was used to represent the test temperature.

Post-test processing. - At the conclusion of the tests, the capsules were allowed to cool to room temperature, pierced by drilling, and drained of the mercury. The capsules were cut lengthwise along the axis, and residual mercury was removed by vacuum evaporation.

One section of each capsule was mounted and examined metallographically in the etched and unetched conditions. Depths of corrosion penetration were measured with a filar eyepiece. Specimens of particular interest were analyzed by means of an electron-beam probe microanalyzer to determine the elemental composition of the corroded areas. Selected corrosion deposits were analyzed chemically to determine their composition.

From P39

Results

Test data. A summary of test conditions, maximum corrosion-penetration depths, and appearance of the corrosion-zone structure is given in table III.

23

7

TABLE III. - REFLUX CAPSULE TEST DATA

SICROMO-9M

Capsule	Temperature °F	Temperature °K	Test time, hr	Maximum depth of attack in.	Maximum depth of attack m	Corrosion manifested as -
1	1000	811	308	0.05×10⁻³	0.13×10⁻⁵	Grain-boundary penetration
2			308	.12	.31	
3			1007	.49	1.24	
4			1007	.51	1.30	
5			2022	.39	.99	
6			4993	1.28	3.25	
7			4993	1.72	4.37	
8	1100	866	305	0.17×10⁻³	0.43×10⁻⁵	Grain-boundary penetration
9			305	.29	.73	
10			1005	.90	2.29	
11			1007	.61	1.55	
12			1007	.73	1.85	
13			2022	1.72	4.37	
14			2022	1.50	3.81	
15			5000	2.14	5.44	
16			4993	2.68	6.81	
17	1150	894	294	0.36×10⁻³	0.91×10⁻⁵	Grain-boundary penetration
18	1150	894	294	.51	1.30	
19	1200	922	211	.49	1.24	
20			290	.56	1.42	
21			305	.63	1.60	
22			305	.75	1.91	
23			1005	1.31	3.33	
24			1007	.92	2.34	
25			1007	1.09	2.77	
26			2022	2.25	5.72	
27			2022	2.12	5.38	
28			5000	3.01	7.65	
29			4993	3.63	9.22	

AM-355

Capsule	Temperature °F	Temperature °K	Test time, hr	Maximum depth of attack in.	Maximum depth of attack m	Corrosion manifested as -
1	1100	866	1004	0.34×10⁻³	0.86×10⁻⁵	Wall recession
2	1100	866	1005	.44	1.12	
3	1200	922	1004	.83	2.11	
4	1200	922	1004	.68	1.73	
5	1200	922	1005	.90	2.29	
6	1300	977	1004	1.12×10⁻³	2.84×10⁻⁵	Wall recession
7	1300	977	1004	1.17	2.97	Wall recession

H-8187

Capsule	Temperature °F	Temperature °K	Test time, hr	Maximum depth of attack in.	Maximum depth of attack m	Corrosion manifested as -
1	1100	866	303	1.29×10⁻³	3.28×10⁻⁵	Porous region
2			1004	1.48	3.76	
3			2022	1.80	4.57	
4			2022	4.25	10.80	
5			4993	3.43	8.71	Fractured porous region
6			4993	4.32	11.00	Fractured porous region
7	1200	922	303	1.14×10⁻³	2.90×10⁻⁵	Porous region
8			2022	4.82	12.20	Fractured porous region
9			2022	4.55	11.60	
10			4993	10.33	26.20	
11			4993	5.30	13.50	
12	1300	977	303	1.36×10⁻³	3.45×10⁻⁵	Porous region
13			303	1.80	4.57	Porous region
14			1004	2.42	6.14	Fractured porous region
15			1004	2.04	5.18	
16			2012	5.82	14.80	
17			2012	7.93	20.10	
18			4622	21.70	55.10	
19			4993	18.38	46.68	

HS-25

#				$\times10^{-3}$	$\times10^{-5}$	
1	1000	811	309	0.46×10^{-3}	1.17×10^{-5}	Porous region →
2	1100	866	294	.85	2.16	
3		→	294	1.00	2.54	
4			294	1.12	2.84	→
5			990	2.79	7.09	
6			1005	3.06	7.77	Fractured porous region
7			2010	3.09	7.85	Fractured porous region
8		→	4002	7.17	18.20	Fractured porous region
9			5000	10.33	26.24	
10	1200	922	27	0.53×10^{-3}	1.35×10^{-5}	Porous region →
11			50	.53	1.35	
12			100	1.04	2.64	
13			305	1.02	2.59	
14			306	1.29	3.28	→
15			306	1.34	3.40	
16			1005	4.69	11.90	Fractured porous region →
17			2010	4.74	12.00	
18		→	2710	9.99	25.40	
19			5000	9.99	25.40	
20	1300	977	50	0.41×10^{-3}	1.04×10^{-5}	Porous region →
21			100	.75	1.91	Porous region
22			305	5.03	12.80	Fractured porous region →
23			2010	21.90	55.60	
24			4002	33.00	83.80	
25			4398	32.80	83.30	
26			5000	34.10	86.60	

AM-350

#				$\times10^{-3}$	$\times10^{-5}$	
30	1250	950	294	0.78×10^{-3}	1.98×10^{-5}	Grain-boundary penetration →
31	1250	950	294	.83	2.11	
32	1300	977	16	.17	.43	
33	1300	977	49	.27	.69	
1	1100	866	295	0.07×10^{-3}	0.18×10^{-5}	Wall recession →
2		→	295	.27	.69	
3			1999	.32	.81	
4		→	4007	.51	1.30	
5			5015	1.90	4.83	
6	1150	894	306	0.39×10^{-3}	0.99×10^{-5}	Wall recession →
7	1200	922	295	.29	.74	
8			295	.32	.81	
9			301	.41	1.04	
10			311	.39	.99	
11			311	.22	.56	
12			1999	7.00	17.80	
13		→	4007	10.40	26.40	
14			5015	9.80	24.90	
15	1250	950	306	0.56×10^{-3}	1.42×10^{-5}	Wall recession →
16	1300	977	295	.50	1.27	
17			295	.53	1.35	
18			311	.90	2.29	
19			311	.49	1.24	
20			1999	7.60	19.30	
21			4007	15.50	39.40	
22			5015	16.90	42.90	
23		→	5015	16.40	41.70	

Visual analysis. - When it was removed from the capsules following a test, the mercury had a bright, silvery luster. Shortly after exposure to air, the mercury began to discolor, and a sludge appeared on the surface. The fluidity of the freshly drained mercury varied markedly and was dependent on material and test conditions. In all cases, a decrease in fluidity and an increase in sludge formation were associated with an increase in the severity of corrosion attack on the capsule wall in the condensing region and an increased amount of crystalline deposit at the liquid-vapor interface.

In general, freshly sectioned capsules showed complete "tinning" of the wall by the mercury. Crystalline deposits were found along the capsule walls in the liquid section, predominantly at the vapor - liquid pool interface. Qualitatively, there was a close relation between deposit buildup and corrosion penetration of the upper wall. The typical appearance of sectioned capsules following the removal of residual mercury is shown in figure 3.

Material:	SICROMO-9M	AM-350	H-8187	HS-25
Test temperature:	1100° F (866° K)	1300° F (977° K)	1300° F (977° K)	1200° F (922° K)
Test period:	5000 hours	2000 hours	5000 hours	5000 hours

C-67-3799
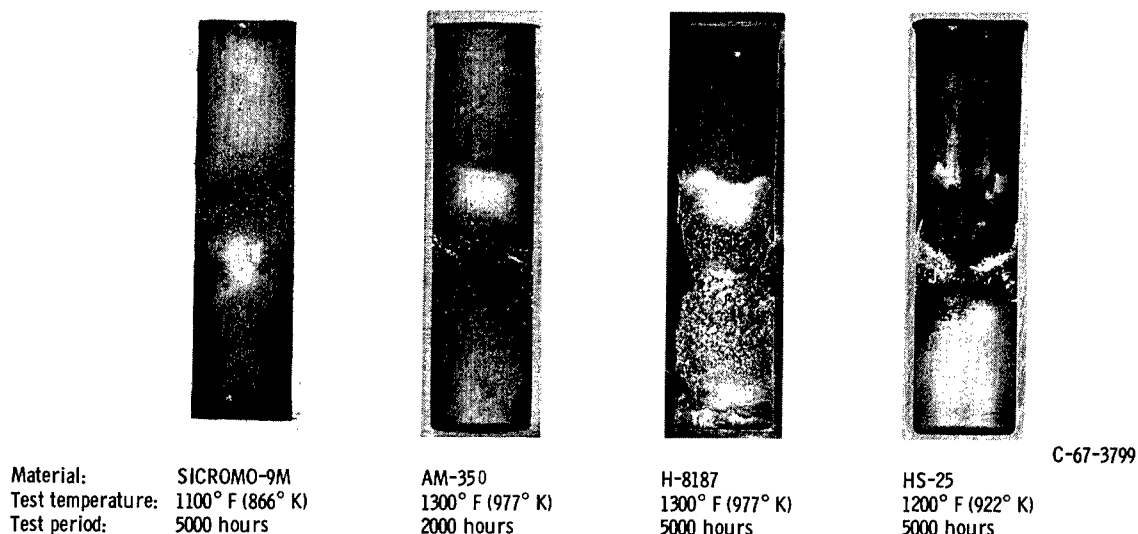
Figure 3. - Typical appearance of sectioned capsules after removal of mercury.

Metallographic analysis. - The maximum corrosion attack always occurred in the upper portion of the capsules. The variation of corrosion penetration down the capsule wall was wedgelike; penetration decreased in a regular manner from the top to the liquid pool (fig. 4). In general, examination of the corroded areas revealed no aberrations (i. e., no localized region of attack with penetration much greater or much less than the surrounding region). The exceptions to this were the AM-350 and AM-355 alloys. In some instances, occasional localized deep penetrations were observed. These anomalous penetrations were disregarded in estimating maximum corrosion penetration.

4x10^{-3} in.
(1x10^{-2} cm)

Corrosion zone

Bulk metal

5.2x10^{-2} in.
(1.3x10^{-1} cm)

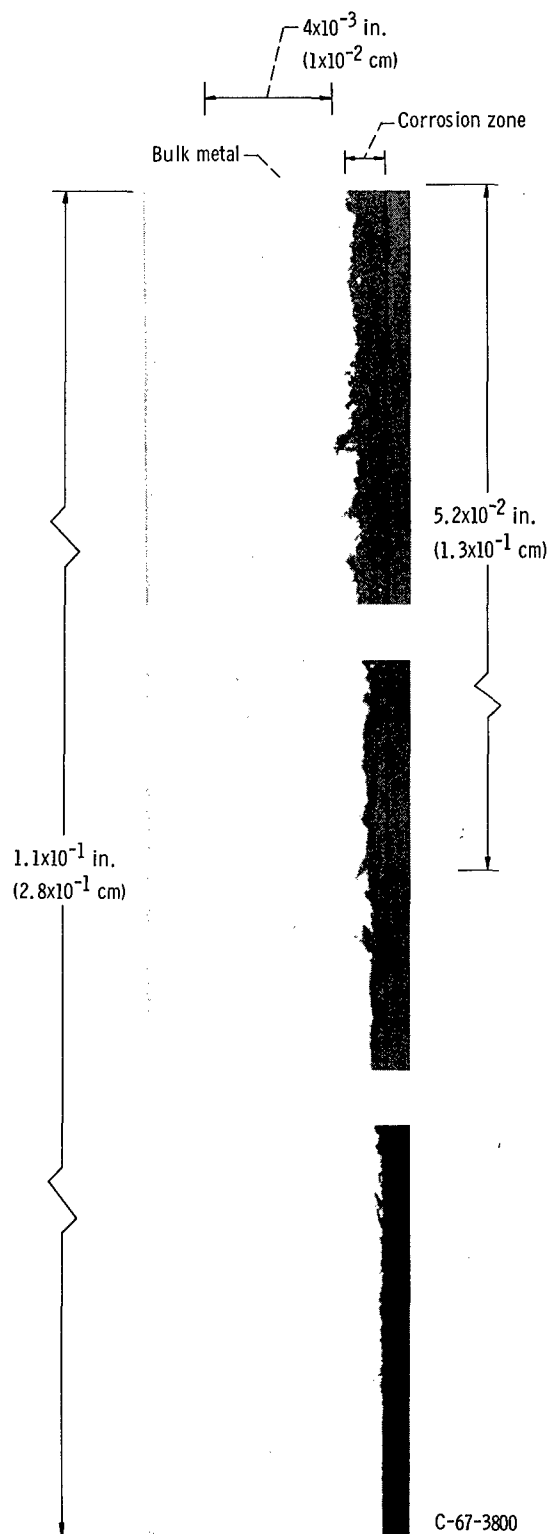1.1x10^{-1} in.
(2.8x10^{-1} cm)

C-67-3800

Figure 4. - Typical variation of corrosion penetration down capsule wall. Photomicrographs of longitudinal section of capsule wall: HS-25; test temperature, 1100° F (866° K); test time, 990 hours; unetched.
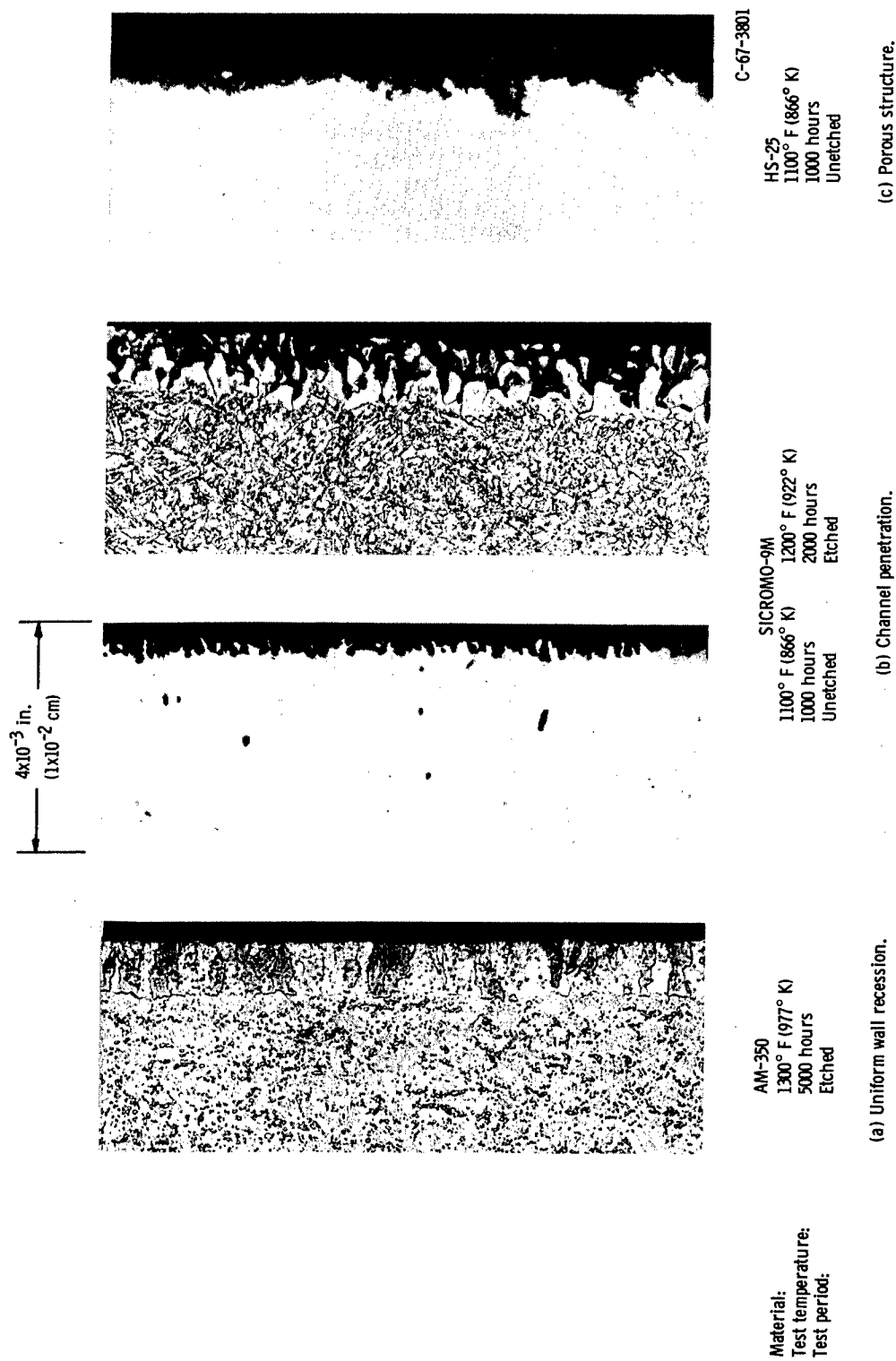
C-67-3801

Material:
Test temperature:
Test period:

AM-350
1300° F (977° K)
5000 hours
Etched

(a) Uniform wall recession.

SICROMO-9M
1100° F (866° K)   1200° F (922° K)
1000 hours   2000 hours
Unetched   Etched

(b) Channel penetration.

HS-25
1100° F (866° K)
1000 hours
Unetched

(c) Porous structure.

4x10⁻³ in.
(1x10⁻² cm)

Figure 5. – Typical appearance of mercury-corroded areas. Photomicrographs of longitudinal section of capsule wall. (Capsule inner wall surface at far right of each photomicrograph.)

The corroded areas presented one of four typical appearances: (1) uniform wall recession, approximately a 130° groove angle at surface grain boundaries (e.g., AM-350, fig. 5(a)), (2) channel-like perforation, approximately a 50° groove angle at surface grain boundaries (e.g., SICROMO-9M, fig. 5(b)), (3) a fine porous structure (e.g., HS-25 and H-8187, fig. 5(c)), and (4) a multifractured porous structure (e.g., HS-25, and H-8187, fig. 3). The groove angles given are approximate, inasmuch as grain-edge rounding and groove asymmetry precluded accurate angle measurements.

All materials except AM-350 and AM-355 showed a progressive change of the form of the corrosion-affected zone with increasing test time and temperature. The HS-25 and H-8187 corrosion zones progressed from a smooth wall to a porous structure and finally to a multifractured porous structure. The SICROMO-9M corrosion zones progressed from a smooth wall to grain-boundary penetrations which deepened and broadened with increasing time and temperature. For the SICROMO-9M alloy, in addition to the gross changes in the corrosion zone, grain transformations were noted (fig. 5(b)). Although extensive wall recession was measured, the corrosion-affected zone of the AM-350 and AM-355 alloys showed little change from the initial smooth wall condition other than a slight surface roughening and grain transformation in a narrow region, 1×10^{-3} inch (2.5×10^{-3} cm) wide, adjacent to the alloy-condensate interface.

Composition of corrosion zones, deposits, and bulk alloys. - The compositions of the corrosion zones, the deposits, and the bulk alloys were determined by one or more of the following techniques: electron-beam microanalysis, chemical analysis, and X-ray diffraction.

Typical corrosion zone compositions were determined for the alloys SICROMO-9M, AM-350, H-8187, and HS-25 by electron-beam microanalysis scans across the appropriate region of selected samples. The SICROMO-9M analysis (fig. 6(a)) shows no effective compositional change in the corrosion zone from that of the bulk alloy. The analysis of AM-350 (fig. 6(b)) shows a depletion of manganese (Mn), chromium (Cr), and nickel (Ni) in the region adjacent to the alloy-condensate interface. Depletion of Ni, Cr, and to a lesser extent cobalt (Co), with a corresponding enrichment of tungsten (W), is shown by the analyses of H-8187 and HS-25 (figs. 6(c) and (d)). The compositions of the corrosion zones of HS-25 and H-8187, as indicated by the electron-beam microanalyses, are listed in table IV. Since the electron-beam analyses of these two alloys account for less than 85 percent of the material, other means (discussed in the following paragraphs) were used to establish the composition of the corrosion zones.

X-ray diffraction patterns were obtained from the corrosion zones of selected HS-25 and H-8187 capsules. These patterns indicate the presence of the intermetallic compounds Co_3W and Co_2W. Patterns obtained from either the as-received material or non-corroded areas of the test capsules do not indicate the presence of Co_3W or Co_2W.
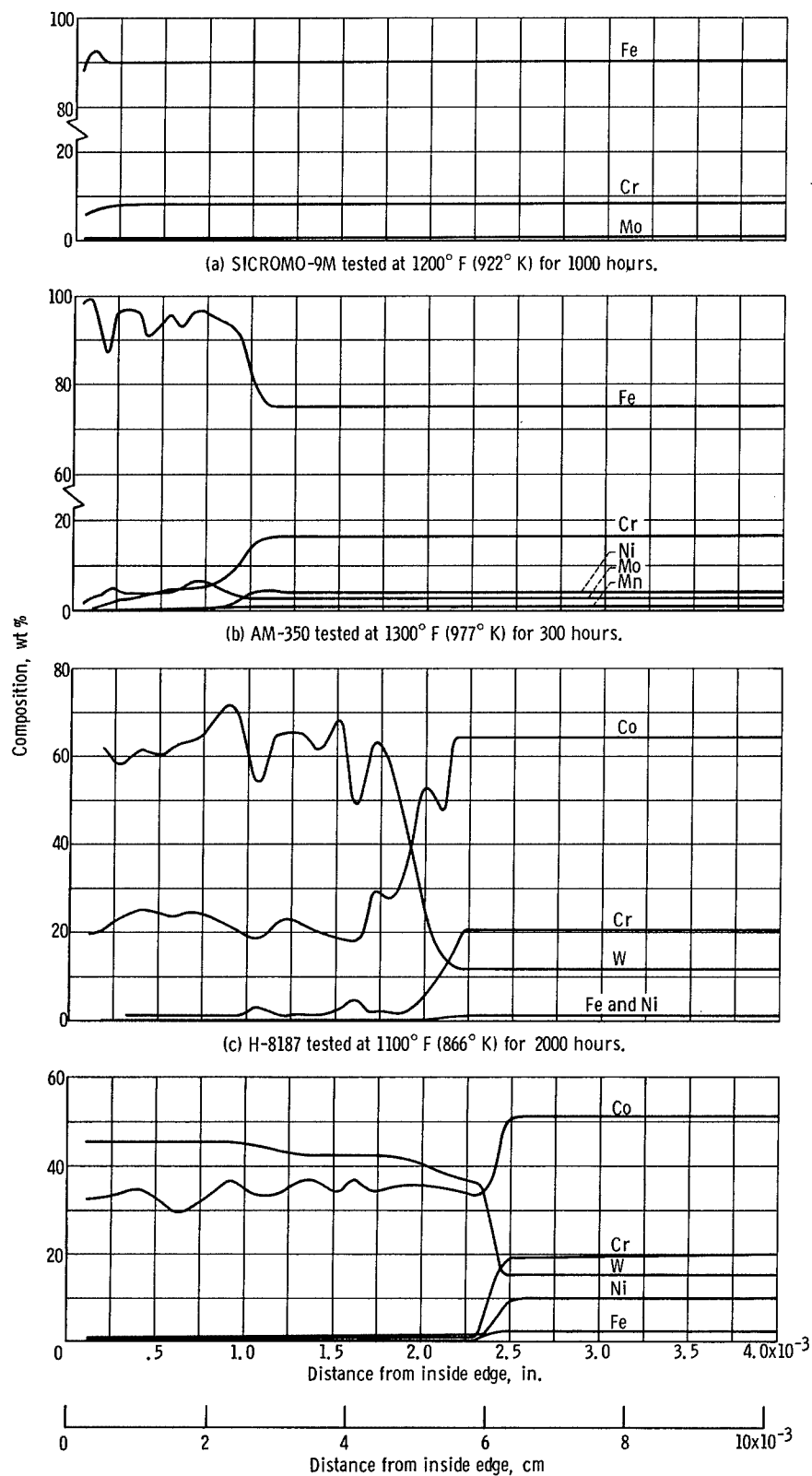
(a) SICROMO-9M tested at 1200° F (922° K) for 1000 hours.

(b) AM-350 tested at 1300° F (977° K) for 300 hours.

(c) H-8187 tested at 1100° F (866° K) for 2000 hours.

(d) HS-25 tested at 1100° F (866° K) for 300 hours.

Figure 6. – Electron-beam microanalysis of corrosion zone and matrix.

14

TABLE IV. - COMPOSITION OF BULK ALLOY, CORROSION ZONE,

AND CORROSION DEPOSITS

Material	Analysis	Co	Fe	Ni	Cr	Mn	W	Mo	N + C
		wt. %							
HS-25									
Bulk	Chemical[a]	51.1	2.5	9.9	19.8	1.2	15.5	---	---
Deposits	Chemical[a]	53.7	2.7	14.5	27.0	1.4	1.7	---	---
Corrosion zone	Electron beam[b]	35	1	0	1	---	44	---	---
	Mass balance[c]	44	---	----	----	---	56	---	---
H-8187									
Bulk	Chemical[a]	64.6	1.1	1.2	20.6	0.6	11.8	0.1	---
Deposits	Chemical[a]	69.0	1.3	1.4	26.7	.6	2.4	.2	---
Corrosion zone	Electron beam[b]	23	0	0	2	---	60	---	---
	Mass balance[c]	44	---	---	----	---	56	---	---
SICROMO-9M									
Bulk	Chemical[a]	----	90.3	----	8.6	0.5	----	0.6	---
Deposits	Chemical[a]	----	87.5	----	7.6	---	----	.3	---
AM-350									
Bulk	Chemical[a]	----	75.1	4.1	16.6	1.1	----	2.9	0.2
Deposits	Chemical[a]	----	69.2	5.4	22.5	.8	----	.4	---

[a]Analyses performed on deposits of capsules 19, 10, 28, and 23, respectively, for HS-25, H-8187, SICROMO-9M, and AM-350.

[b]Analyses performed on corrosion zone of capsules 4, 3, 23, and 18, respectively, for HS-25, H-8187, SICROMO-9M, and AM-350.

[c]Calculated from composition of bulk and deposits and assumption of conservation of mass.

TABLE V. - CALCULATED FLUID PARAMETERS FOR REFLUX

CAPSULE TESTS

Capsule bottom temperature		Mercury vaporization rate		Mercury film thickness		Average mercury film velocity	
°F	°K	in.^{3}/hr	m^3/hr	in.	m	in./sec	m/sec
1000	811	0.34	0.51×10^{-5}	0.39×10^{-3}	0.99×10^{-5}	0.18	0.46×10^{-2}
1100	866	.45	.67	.43	1.1	.22	.56
1200	922	.62	.92	.47	1.2	.27	.69
1300	977	.84	1.4	.54	1.4	.35	.89
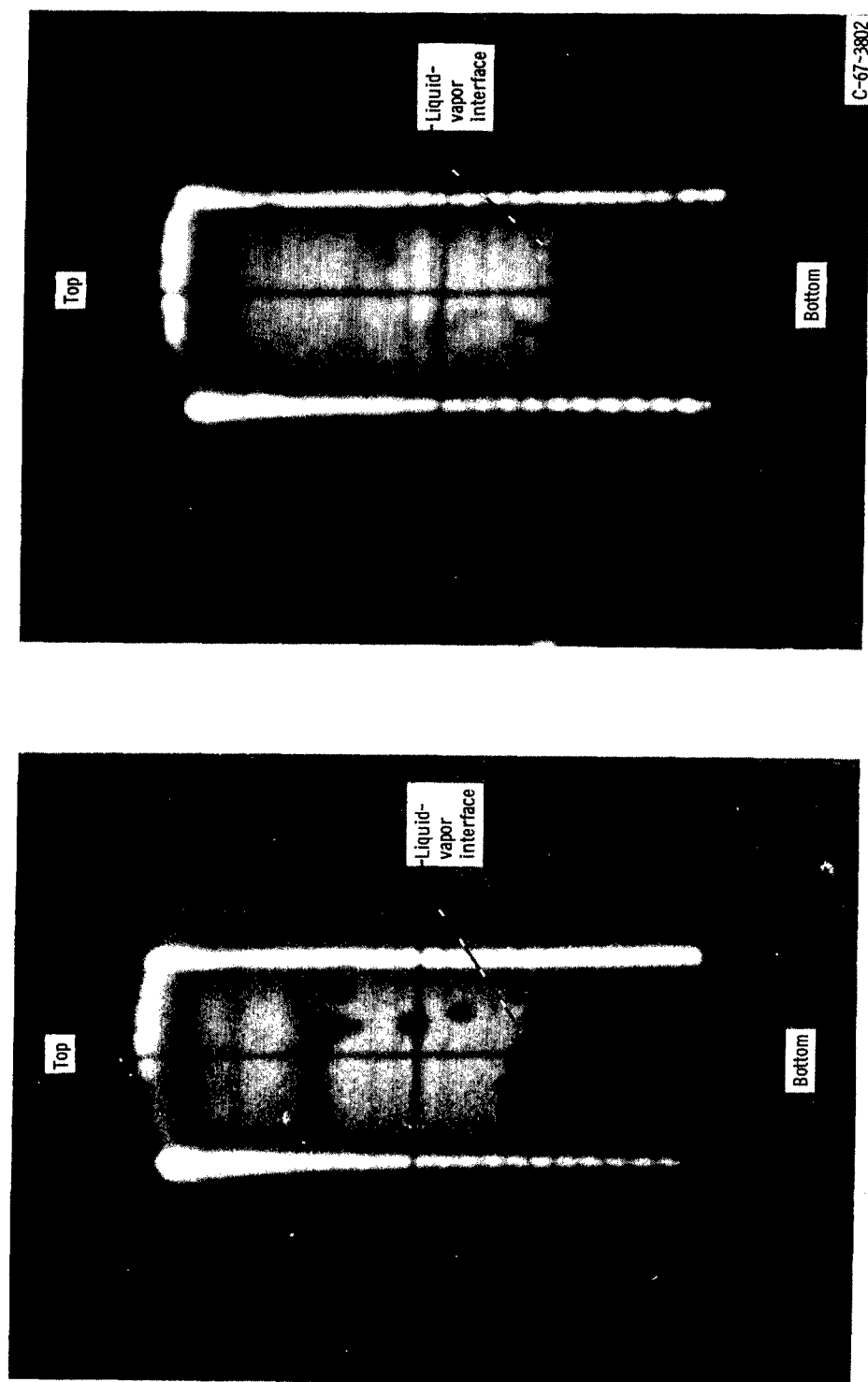
(a) At 5 hours of test time.

(b) At 20 hours of test time.

Figure 7. – Interior of SICROMO-9M reflux capsule during testing at 1200° F (923° K). Single frame of 16 millimeter film; 16 frames per second through X-ray-image amplifier.

Chemical analyses were made of the bulk alloys SICROMO-9M, AM-350, AM-355, H-8187, and HS-25 and of deposits from selected test capsules of SICROMO-9M, AM-350, H-8187, and HS-25. The results are given in table IV. In all cases, except for SICROMO-9M, there was an enrichment of the more soluble elements, Ni, Cr, or Mn, in the deposits as compared with the bulk alloy. In the case of SICROMO-9M, the deposits were approximately the same composition as the bulk alloy.

A mass balance calculation was made of the weight percentage of W and Co remaining in the HS-25 and H-8187 corrosion zones by using the elemental composition data for the bulk alloy and the corrosion deposits. The following assumptions were made: (1) all material removed from the corrosion zone became deposits and (2) the amount of elements other than W and Co in the corrosion zone were negligible. Listed in table IV are the mass balance estimates of the weight percentages of W and Co in the HS-25 and H-8187 corrosion zones. The Co-W ratio, based on the mass balance estimates, is 2.5 for both materials. This ratio is consistent with the X-ray diffraction results, which indicated the presence of both Co_3W and Co_2W as the major corrosion zone constituents.

Mercury vaporization rate and condensate film properties. - Table V presents the calculated values of the mercury vaporization rate and condensate film thickness and velocity for capsule temperatures of 1000°, 1100°, 1200°, and 1300° F (811°, 866°, 922°, and 977° K). Details of the calculation are discussed in appendix A.

With the aid of an X-ray image amplifier the course of the mercury condensation process was followed in a typical capsule at 1200° F (922° K) over a period of 580 hours. During the first 16 hours of operation dropwise condensation was noted (fig. 7(a)). Drops formed and grew at preferential sites along the upper portion of the capsule and periodically ran down the wall. After 16 hours no drops were observed; the upper portion of the capsule appeared to be of more or less uniform density as viewed through the X-ray image amplifier (fig. 7(b)). Mercury condensation apparently occurred uniformly near the top of capsule and the condensate traveled down the capsule wall in film flow. An estimation of the film thickness of the mercury condensate, based on a comparative optical density measurement with a known thickness of lead used as the standard, indicated the film thickness to be less than 1×10^{-3} inch (2.5×10^{-3} cm). This thickness is to be compared with the calculated film thickness, 5×10^{-4} inch (1.27×10^{-3} cm).

ANALYSIS

In this investigation an attempt was made to identify, for each material tested, the probable rate-controlling step at any time during the progress of corrosion. The method of identification of rate-controlling step was based on a comparison of the experimental kinetic constants b_r and ΔH_r, respectively, with the theoretical kinetic constants b_i

and ΔH_i for each of i steps of a proposed corrosion model. Agreement of the theoretical kinetic constants of a particular step with the respective experimental kinetic constants was taken to infer that that step was rate determining. In the following presentation, the experimental kinetic constants for each alloy were obtained by a regression analysis data-fitting technique. The theoretical kinetic constants associated with proposed corrosion models were derived from transport theory relations for the pertinent boundary conditions.

The possibility of mechanism changeover (i. e., change of rate-controlling step) during the course of the corrosion tests is also evaluated. This possibility is assessed (1) from the experimental results by means of data grouping and statistical testing and (2) from a theoretical consideration of the corrosion models.

Experimental Kinetic Constants

Criterion for corrosion attack. - The capsule method of corrosion testing precludes the use of weight change as the corrosion criterion. Therefore, in this study, maximum corrosion penetration was used as the sole measure of corrosion attack. Two assumptions were made in applying this criterion:

(1) Penetration is proportional to the corrosion weight change.

(2) The test material is relatively homogeneous from the point of view of corrosion attack (i. e., there are no local regions of high corrosion susceptibility such as microcracks or soluble constituent concentrations).

The first assumption is validated, at least in the case of attack leading to uniform wall recession, by the principle of the conservation of mass; it also finds support in the general observation of increasing corrosion deposit with increasing penetration. The second assumption is supported by the fact that except for AM-350 and AM-355 alloys, no abnormal localized regions of penetration were found in the corroded areas of the test capsules. In the case of AM-350 and AM-355, where occasional deep localized penetrations were observed, the anomalous penetrations were disregarded in estimating maximum penetration.

Data-fitting techniques. - Corrosion data, as a function of time and temperature, are customarily fitted to the empirical relations:

$$p_r = k_r t^{b_r} \tag{5}$$

$$\log k_r = a_r + \frac{B_r}{T} \tag{6}$$

where p_r is corrosion penetration (or weight loss), T is the test temperature on the absolute scale, t is time, and k_r, a_r, b_r, and B_r are constants. The time law (i. e., the relation between p_r and t at constant temperature T) is termed linear when $b_r = 1$ and parabolic when $b_r = 1/2$. The constant B_r in the Arrenhius relation (eq. (6)) is proportional to the activation energy of the overall corrosion reaction (viz, $\Delta H_r = 4.58 \times 10^{-3} B_r$ kcal/mole (19.2 B_r J/mole)).

When the test data are fitted to equations (5) and (6) by simple linear regression (least-squares method), the determination of b_r and B_r is laden with certain difficulties. First, the precision of determination of b_r and B_r is generally poor because the dependent variable p_r, as a result of uncontrolled or unknown experimental factors, invariably has a large random error (even though the independent variables t and T may have relatively small errors of measurement). Second, and perhaps as significant, simple linear regression analysis of the experimental data yields values for b_r and B_r which are dependent, respectively, on the values chosen for t and T (i. e., dependent on the arrangement of the experimental observations, ref. 7).

These difficulties can be minimized or avoided to some extent by the use of multiple linear regression analysis (ref. 7). A single regression equation containing all the independent variables is used to express the dependent variable. By addition of independent variables to the regression equation, it is possible to account for some of the unexplained variation in the dependent variable obtained by simple linear regression analysis. This resulting increase in the precision of estimate of the dependent variable p is preferred when analyzing data which exhibit large scatter, such as in the present case. Additionally, multiple linear regression analysis affords a more exact basis for estimating b_r and B_r than simple linear regression and also serves to summarize the results of a large number of observations in a single convenient statement.

It must be emphasized that a statistical analysis of the data does not miraculously transform "bad" data into "good" data. The purpose in this analysis is to obtain the best possible estimate of the dependent variable and the kinetic constants. The uncertainty in the estimates must always be kept in mind and continually viewed with reference to a pertinent error statistic.

Analysis of the test data by multiple linear regression. - The corrosion data were treated by the technique of multiple linear regression. The Regression Analysis Program with Iterative Evaluation of Relations (RAPIER) (an unpublished computer program written by Bert Henry, Steven M. Sidik, and R. Lambird of Lewis) was used. The estimating equation used was obtained by combining equations (5) and (6) as follows:

$$\log p_r = a_r + b_r \log t + \frac{B_r}{T} \tag{7}$$

TABLE VI. - RESULTS OF MULTIPLE LINEAR REGRESSION ANALYSES

Material	Data [a]	Data points	Regression coefficients			Standard deviation of regression coefficients			Standard error of estimate of log p_r, $s_{log\ p_r}$	Residual error variance, $s^2_{log\ p_r}$	Coefficient of multiple determination[b], R^2_m
			a_r	b_r	B_r	s_{a_r}	s_{b_r}	s_{B_r}			
HS-25	Total	26	2.5731	0.79114	-3951.9	0.6142	0.0466	554.6	0.162	0.0263	0.94
	Group 1	15	.5458	.58342	-1712.7	.7945	.0896	814.2	.137	c .0200	.80
	Group 2	19	2.7311	.92504	-4506.8	.6918	.0576	662.0	.145		.94
SICROMO-9M	Total	33	2.4707	0.73534	-4185.2	0.4332	0.0460	417.8	0.140	0.0196	0.90
	Group 1	22	3.2780	.98216	-5469.8	.5299	.0814	551.9	.128	c .0107	.89
	Group 2	20	.6992	.58536	-2159.1	.3564	.0338	379.1	.067		.97
H-8187	Total	19	1.1873	0.68338	-2609.7	0.3794	0.1043	822.1	0.199	0.0396	0.76
	Group 1	11	-.1207	.54068	-1037.4	.2286	.1283	817.0	.142	c .0250	.69
	Group 2	14	1.2923	1.01128	-3744.5	.3222	.1892	871.3	.169		.77
AM-350[d]	Total	30	3.7425	1.0659	-6380.2	0.6461	0.0948	911.2	0.247	0.0609	0.86

[a] Group 1, Data exhibit initial corrosion structure; group 2, Data exhibit succeeding corrosion structure.

[b] R^2_m = Sum of squares due to multiple regression/Total sum of squares of log p_r values about their mean.

[c] Pooled residual error variance estimate = $SS_1 + SS_2 / df_1 + df_2$, where SS_j is residual sum of squares for jth data group and df_j is degrees of freedom.

[d] AM-350 and AM-355 data combined.

The units arbitrarily selected for the variables were as follows: p_r, inch$\times 10^{-3}$; t, hours; T, $^{\circ}$K.

The results of the regression analyses are presented in table VI. The data were grouped in the following categories: total, group 1, and group 2. The latter two categories are discussed in the next section. The 23 AM-350 and the 7 AM-355 data points were treated as one data set, since compositionally and structurally AM-350 and AM-355 are almost identical.

It is apparent from table VI that for the total data (i.e., all the data points for a given material) the values of the coefficient of multiple determination R_m^2 are large and range from 0.76 to 0.94. The large values for R_m^2 indicate that the functional relations selected for the variables were reasonably good choices, in that $\left(R_m^2 \times 100 \right)$ percent of the variation in the dependent variable p can be accounted for when the data are fitted to equation (7).

Taken by themselves, the values obtained from the total data for B_r ranging from -2610 to -6380, which correspond to ΔH_r values of -12.0 to -29.2 kilocalories per mole (-5.02$\times 10^4$ to -1.22$\times 10^5$ J/mole), appear to be reasonable for this coefficient. However, except for AM-350, the values obtained for b_r do not correspond to those associated with the expected processes, namely, boundary or diffusional processes which have linear or parabolic time-law relations, respectively. The b_r values (0.79, 0.74, and 0.68 for HS-25, SICROMO-9M, and H-8187) lie between the expected singular values of 1 or 0.5.

Mechanism changeover. - It is probably more than coincidental that the materials for which anomalous values of b_r are found also exhibit marked changes in the structure of the corrosion zone with increasing time and temperature. Oxidation studies indicate that mechanism changes occur as a consequence of changes in oxide-layer thickness or oxide-layer adherence. Analogously, it may be expected that growth or alteration of the corrosion zone may change the nature of the material-transport path and, hence, result in a change of corrosion mechanism. If, in fact, the rate process changes during the course of a test, for example from linear to parabolic, then the value of b_r derived from the total test data would assume some average value $\bar{b}_r$, where $1 > \bar{b}_r > 0.5$.

The hypothesis that changes in the thickness or structure of the corrosion zone are accompanied by changes in corrosion mechanism was tested as follows. First, the corrosion data for each material were grouped according to the corrosion-zone criterion as described later in this section. Second, a multiple linear regression analysis was performed on each data group. Third, the grouped-data analyses were compared to the analyses previously performed on the total data. For each material, data exhibiting the initial corrosion structure were designated as group 1 and those exhibiting the succeeding structure as group 2. Data falling within the corrosion structure region of transition were included in both group 1 and group 2. The grouping criterion is as follows:

(1) SICROMO-9M

    (a) Group 1, superficial penetrations, $< 1 \times 10^{-3}$ inch (2.5×10^{-3} cm)

    (b) Group 2, deep penetrations, $> 1 \times 10^{-3}$ inch (2.5×10^{-3} cm)

(2) HS-25 and H-8187

    (a) Group 1, porous structure

    (b) Group 2, multifractured porous structure

The results of the grouped-data analyses for HS-25, SICROMO-9M, and H-8187 are given in table VI.

A goodness-of-fit criterion is needed to compare the grouped-data analyses with the total-data analyses. The coefficient of multiple determination R_m^2, a measure of the proportion of the variation in the dependent variable explained by the regression equation, was used to validate the choice of functional relations for the variables. This coefficient is a relative measure of goodness of fit. However, once the form of the estimating equation is found to be satisfactory, an absolute measure of goodness of fit should be used for comparison of analyses employing the same estimating equation. Therefore, the residual error variance (ref. 7), a measure of the closeness with which the estimated values of the dependent variable agree with the experimental values, is employed herein as the comparison criterion for the variously grouped data.

An inspection of the values of residual error variance $s_{\log p_r}^2$ shows that grouping the data according to corrosion structure has in all cases significantly improved the precision in the determination of $\log p_r$. Although grouping of the SICROMO-9M data into groups of superficial penetration ($< 1 \times 10^{-3}$ in. (2.5×10^{-3} cm)) and deep penetration ($> 1 \times 10^{-3}$ in. (2.5×10^{-3} cm)) was arbitrary, it fortuitously proved to be a good choice. Trial analyses performed on the SICROMO-9M data (not shown in table VI) yielded a poorer fit of the data when values either slightly greater or slightly less than 1×10^{-3} inch were used to define the division between superficial and deep penetration.

Best estimate of regression coefficients. - The grouped data for HS-25, H-8187, and SICROMO-9M give values of b_r that closely approximate the expected kinetic values of 1.0 or 0.5 and also yield reasonable values of ΔH_r. In view of this and since data grouping can be rationalized on both a structural and a statistical basis, the best estimates of the coefficients of equation (7) were considered to be those from the grouped-data analyses.

For AM-350 no breakdown of the data into groups was warranted. In this instance, for the total data the value of b_r obtained was approximately 1. Further, no marked changes were observed in the AM-350 corrosion zone over the time and temperature range of the tests. The coefficients for AM-350, therefore, were considered to be those for the total data (table VI).

For later comparison of results, the best-estimate values of b_r and ΔH_r and their standard deviations are listed in table VII.

TABLE VII. - EXPERIMENTAL KINETIC CONSTANTS

Material	Data	Time-law constant, b_r	Activation energy, $-\Delta H_r$	
			kcal/mole	J/mole
HS-25	Group 1	0.58±0.09	7.8±3.7	33±16×10³
	Group 2	.93±0.06	20.6±3.0	86±13
SICROMO-9M	Group 1	.98±0.08	25.0±2.5	105±11
	Group 2	.59±0.03	9.9±1.7	41±7
H-8187	Group 1	.54±0.13	4.8±3.7	20±16
	Group 2	1.01±0.19	17.1±4.0	72±17
AM-350	Total	1.07±0.09	29.2±4.2	123±17

Theoretical Kinetic Constants

Proposed corrosion models. - Two corrosion models are presented. Each proposed model fits one of the two general modes of corrosion attack observed in the test capsules, namely, uniform attack or selective attack. In these models, movement of atoms from the bulk solid material to the bulk liquid mercury occurs through a series of consecutive and parallel material-transport steps.

In the following presentation, S_i is used to designate the ith step and $S_{i,k}$ is used to designate the kth parallel path for the ith step. Shown in figure 8(a) is a schematic representation of the transport steps proposed for the selective attack model:

(1) Diffusion in the solid S_1, consisting of the parallel steps, volume diffusion $S_{1,1}$ and grain-boundary diffusion $S_{1,2}$

(2) Solution S_2, consisting of the parallel steps, grain solution $S_{2,1}$ and grain-boundary solution $S_{2,2}$

(3) Diffusion in a static liquid S_3

(4) Convective diffusion S_4

Figure 8(b) illustrates the transport steps proposed for the uniform attack model (viz, S_1, S_2, and S_4)

General conditions and assumptions. - During a test, mercury vapor condenses continuously near the top of the capsule (see fig. 9). The condensate flows down the capsule wall as a thin film in laminar steady-state flow and enters the liquid pool at $y = -l$. It was assumed that condensation at the mercury film - mercury vapor interface $x = h$ is negligible. Since the measured temperature variation along the upper capsule wall is small and the heat flux is low, the film temperature was assumed to be uniform.
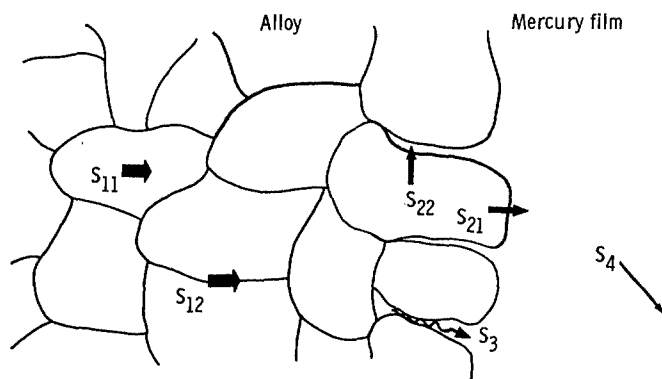
(a) Selective attack model.
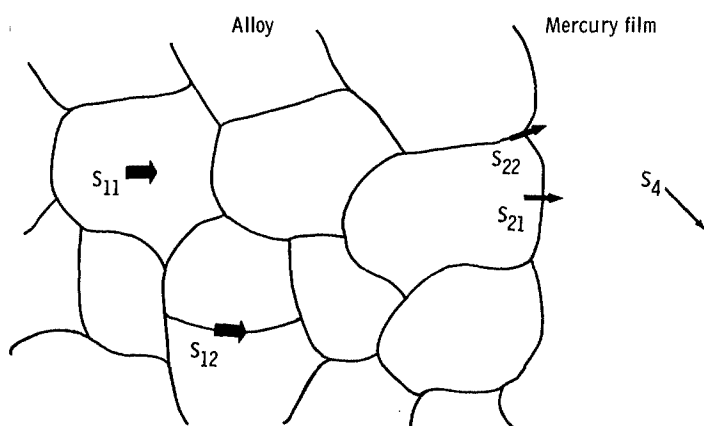
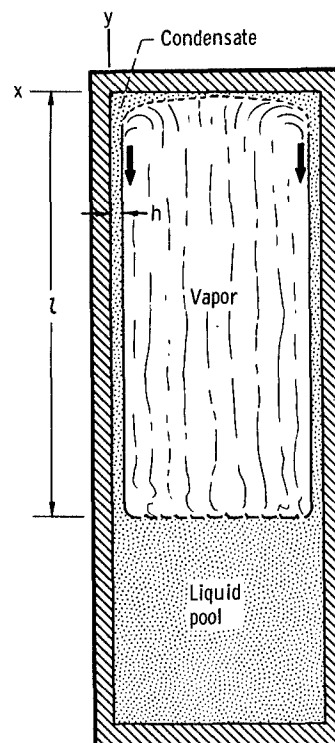(b) Uniform attack model.

Figure 8. - Corrosion models.

Figure 9. - Mercury flow in reflux capsule.

In the region of condensation the concentration of dissolved material was assumed to be approximately 0 (i.e., $c \approx 0$ at $y = 0$). Lastly, it was assumed that steady-state conditions prevail at any point within the mercury film (i.e., $\partial c / \partial t = 0$).

Time-law constant. - A mass-transport - time relation for each step of the proposed models was derived in the form of equation (1) from a consideration of (1) Fick's first and second laws of diffusion, (2) the Navier-Stokes equation, (3) the theory of rate processes, and (4) the conservation of mass. The boundary conditions for each material-transport step are the conditions which prevail when the step under consideration is as-

sumed to be rate controlling. Only the overall step was considered in the derivation of
the time-law constant b_i. Parallel paths were not treated separately, since the mass-
transfer - time relation for each path takes the same form (see appendix B). A summary
of the estimated b_i values for material-transport steps S_1, S_2, S_3, and S_4 is given in
table VIII.

TABLE VIII. - THEORETICAL KINETIC CONSTANTS

Material-transport step	Time-law constant, b_i	Iron-base alloys		Cobalt-base alloys	
		Activation energy, ΔH_i			
		kcal/mole	J/mole	kcal/mole	J/mole
S_1	0.5	30	126×10^3	30	126×10^3
S_2	1.0	11.0	46.0	16.4	68.5
S_3	.5	7.0	29.3	9.7	37.6
S_4	1.0	17.3	72.3	22.7	94.9

Diffusion in the solid S_1: If diffusion through the bulk solid is the rate-controlling
step, and with the assumption that the solid is a semi-infinite medium, the boundary
conditions are as follows:

$$\text{for } t = 0, \ c = c_b \text{ at } x < 0 \text{ and } 0 > y > -l$$

$$\text{for } t > 0, \ c_w \approx 0 \text{ at } x = 0 \text{ and } 0 > y > -l$$

where c_b and c_w are the concentrations in the bulk and at the wall, respectively, of
the diffusing species. The solution of this problem is

$$w_1 = \alpha_1 c_b D_s^{1/2} t^{1/2} \tag{8}$$

where α_1 is a constant, D_s is the diffusion coefficient for the species in the bulk solid
(assumed to be independent of c). For the selective attack model, if it is assumed that
the penetration is proportional to w_1, equation (8) may be written as

$$p_1 = \beta_1 D_s^{1/2} t^{1/2} \tag{9}$$

where p_1 is the penetration and β_1 is the appropriate proportionality constant. For
the uniform attack model, if it is assumed that recession of the wall is proportional to

25

the amount of diffusing substance, solution of the problem of a moving boundary (refs. 8 and 9) leads to a relation identical to equation (9) with the exception that the proportionality constant is different and p_1 represents the amount of wall recession.

Solution S_2: If solution is the rate-controlling step, the boundary conditions for $t > 0$ are $c = c(y)$ at $x = 0$ and $0 > y > -l$. The solute concentration $c(y)$ is a function of y as determined by the convective diffusion parameters of the flowing mercury film. The amount of a given species that passes into solution per unit time per unit surface area of solid is

$$G = k_{sr} \left[c_o - c(y) \right] \tag{10}$$

where k_{sr} is a solution rate constant (a function only of temperature) and c_o is the equilibrium solubility concentration of the solute in mercury.

If the rate of corrosion penetration or wall recession is assumed to be proportional to the flux of atoms through the surface into the mercury, then the surface flux is given by

$$j_{x=0} = \alpha_2 \frac{dp_2}{dt} \tag{11}$$

where α_2 is a proportionality constant and p_2 is the corrosion penetration or wall recession. For steady-state conditions,

$$j_{x=0} = G$$

Equating equations (10) and (11) and integrating with respect to t yield the following kinetic relation for the solution-controlled process:

$$p_2 = \frac{k_{sr}}{\alpha_2} \left[c_o - c(y) \right] t \tag{12}$$

Diffusion in static liquid S_3: If diffusion along quiescent liquid-filled channels or networks is the rate-controlling step, the boundary conditions for $t > 0$ are:

$$c = c_o \text{ at } x = p_3 \text{ and } 0 > y > -l$$

$$c = c'(y) \text{ at } x = 0 \text{ and } 0 > y > -l$$

where p_3 is the depth of greatest penetration of the channel and $c'(y)$ is the solute concentration at the channel mouth (a function of y as determined by the convective diffusion parameters of the mercury film).

The flux of solute from the head to the mouth of the channel is inversely proportional to the length of the diffusion path and directly proportional to the concentration difference as follows:

$$j = \frac{D_l \left[c_0 - c'(y) \right]}{p_3} \tag{13}$$

where D_l is the diffusion coefficient for the solute in mercury assumed to be independent of c.

If the penetration rate is assumed to be proportional to the flux, then

$$j = \alpha_3 \frac{dp_3}{dt} \tag{14}$$

where α_3 is a proportionality constant. Substituting the relation for j of equation (13) into equation (14) and integrating with respect to t result in the kinetic relation for the static liquid-diffusion-controlled process

$$p_3 = \left\{ \frac{2D_l \left[c_0 - c'(y) \right]}{\alpha_3} \right\}^{1/2} t^{1/2} \tag{15}$$

Convective diffusion S_4: If convective diffusion is the rate-controlling step, the boundary conditions for $t > 0$ are, effectively,

$$c = c_0 \text{ at } x = 0 \text{ and } 0 > y > -l$$

and

$$\frac{dc}{dx} = 0 \text{ at } x = h \text{ and } 0 > y > -l$$

The concentration distribution for a solute diffusing through a flowing thin film in laminar flow and steady state is given in reference 10 as

$$3\bar{v}\left(\frac{x}{h} - \frac{x^2}{2h^2}\right)\frac{\partial c}{\partial y} = D_\ell \frac{\partial^2 c}{\partial x^2} \tag{16}$$

where $\bar{v}$ is the average film velocity (eq. (A3)) and h is the film thickness (eq. (A4)). Since the liquid film is flowing at relatively low velocities (see table V), a fully developed diffusion regime will be established across the thickness of the film a short distance from the top of the film. Calculations indicate that the thickness of the diffusion boundary layer becomes comparable to the film thickness at $y \approx 4{\times}10^{-3}$ inch (10^{-2} cm).

The convective diffusion mass transfer problem of S_4 is analogous to the problem of heat transfer to a fluid in laminar flow along a wall which is maintained at uniform temperature. The solution to the heat-transfer problem (ref. 11), when applied to the convective diffusion problem, yields the following expression for the flux of mass at the surface:

$$j_{x=0} = \frac{D_\ell c_o f}{h} e^{-n\xi} \tag{17}$$

for values of ξ greater than 0.12 (i.e., $y > 10^{-2}$ cm) where n and f are constants and $\xi = D_\ell y / 3\bar{v}h^2$.

If it is assumed that the penetration rate is proportional to the flux,

$$j_{x=0} = \alpha_4 \frac{dp_4}{dt} \tag{18}$$

where α_4 is a proportionality constant and p_4 is the penetration. Substituting the expression for the flux (eq. (17)) into equation (18) and integrating with respect to time yield the kinetic relation for the convective diffusion controlled process

$$p_4 = \frac{D_\ell f c_o}{h\alpha_4} e^{-n\xi} t \tag{19}$$

Activation energy. - The activation energy ΔH_i associated with each material-transport step is defined by equation (2). For purposes of evaluating ΔH_i, the differential form of equation (2), namely,

$$\frac{R\, d(\ln k_i)}{d\frac{1}{T}} = \Delta H_i \tag{4}$$

was used. Expressions for k_1, k_2, k_3, and k_4 (multiplied by a proportionality constant) are obtained directly from equations (9), (12), (15), and (19), respectively. The expressions for k_i, evaluated at $y \approx 0$, were introduced into equation (4) and the differential operation was performed. The ΔH_i values obtained are as follows (see appendix C for details of the calculation):

$$-\Delta H_1 = 0.5\ Q_d^A \tag{20}$$

$$-\Delta H_2 = Q_s^A + Q_{sr}^A \tag{21}$$

$$-\Delta H_3 = 0.5 \left(Q_s^A + Q_v + RT \right) \tag{22}$$

$$-\Delta H_4 = Q_s^A + Q_v + 2.75\ RT \tag{23}$$

where Q_d^A is the effective activation energy for chemical diffusivity in alloy A (where A represents any one of the four alloys tested), Q_s^A and Q_{sr}^A are, respectively, the effective activation energy of solution and solution rate in mercury of alloy A, and Q_v is the activation energy for viscous flow in mercury. The average temperature over the experimental range, 900° K, is used for T.

Of the four activation energies only Q_v can be readily estimated. The value of Q_v was assumed to be 1.3 kilocalories per mole (5.4×10^3 J/mole) (ref. 12). Because of the complex nature of the diffusion and solution processes of multicomponent systems, several simplifying assumptions must be made to obtain estimates of Q_d^A, Q_{sr}^A, and Q_s^A. As a result, too much confidence should not be placed in the value calculated for ΔH_i.

The evaluation of Q_d^A was based on the following assumptions:

(1) Volume diffusion $S_{1,1}$ is the predominant mode of diffusion under the test conditions.

(2) The test alloys can be treated as pseudobinary systems (i.e., Co-Cr or Fe-Cr systems).

(3) The thermodynamic activity coefficients of the major constituents of each alloy are effectively constant with change in composition.

The activation energy for volume self-diffusion of the major constituent elements of the test alloys (Fe, Co, Cr) have comparable values (ref. 13) that fall within the range of 60 ± 10 kilocalories per mole ($2.51 \pm 0.42 \times 10^5$ J/mole). Therefore, the value of the effective activation energy of chemical diffusivity for all the test alloys was taken to be approximately 60 kilocalories per mole (2.51×10^5 J/mole).

The evaluation of Q_s^A was based on the following assumptions:

(1) Only the base element of any given alloy (i.e., Fe or Co) need be considered in the solution process.

(2) The influence of mutual solubility effects on the activation energy of solution is negligible.

The first assumption is supported by the fact that the alloy base element was the major component of the corrosion deposits (see table IV). The second assumption is supported by the results of a study of the solubility of the alloys HS-25, H-8187, and SICROMO-9M in mercury (ref. 14).

The data from reference 14 for the cobalt solubility of the alloys HS-25 and H-8187 as a function of temperature are presented in figure 10. Plotted on this same figure are the data from references 15 and 16 for elemental cobalt solubility. The data from reference 14 for iron solubility of the alloy SICROMO-9M are shown in figure 11. Also plotted on figure 11 are the data from references 15 and 17 for elemental iron solubility. Although AM-350 data are given in reference 14, these data are not presented herein be-
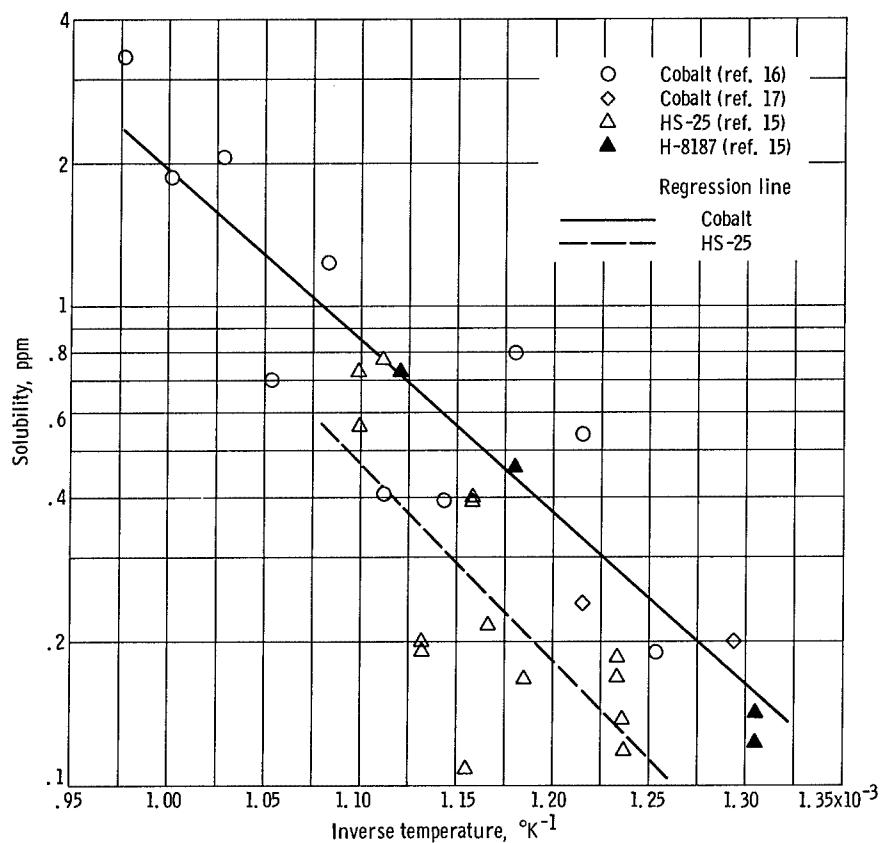
Figure 10. - Solubility of cobalt in mercury. For elemental cobalt, log (ppm Co) = 3.8725 - (3585.3/T); standard deviation of log (ppm Co), 0.1925; standard deviation of slope, 560.8. For cobalt from HS-25, log (ppm Co) = 4.1730 - (4093.4/T); standard deviation of log (ppm Co), 0.2029; standard deviation of slope, 1099.
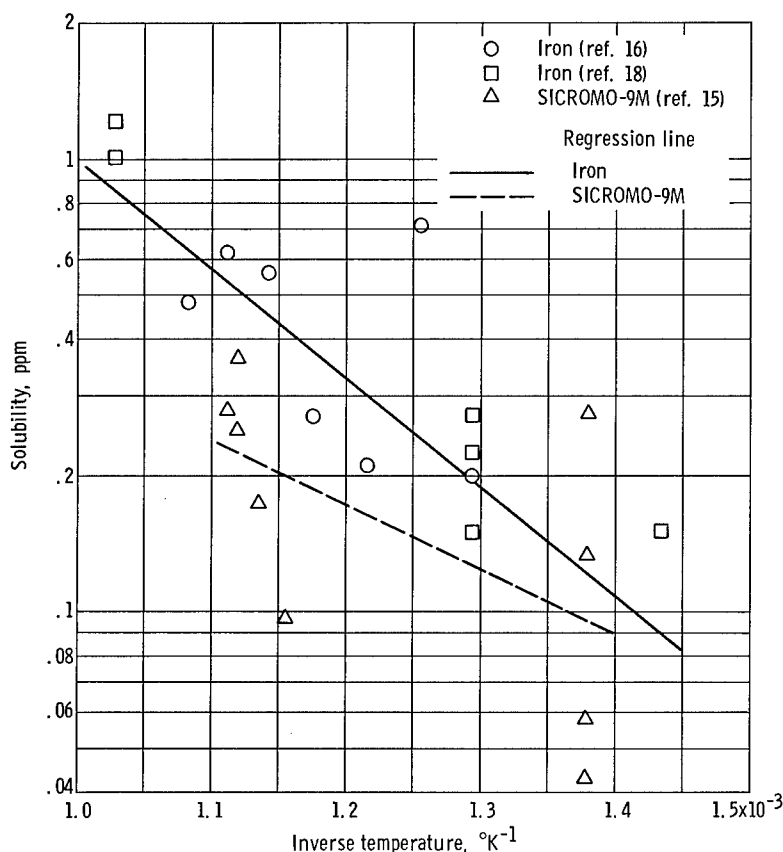
Figure 11. - Solubility of iron in mercury. For elemental iron, log (ppm Fe) = 2.4396 - (2409. 1/T); standard deviation of log (ppm Fe), 0.1911; standard deviation of slope, 453.9. For iron from SICROMO-9M, log (ppm Fe) = 0.9442 - (1426. 1/T); standard deviation of log (ppm Fe), 0.2826; standard deviation of slope, 752.

cause of their extremely large scatter. Our estimates of the regression line and relevant standard deviations for the alloy and element data are shown on each figure. Since there are only four data points for the H-8187 alloy, no regression estimate was made. The slopes of the regression lines shown in figures 10 and 11, when multiplied by the factor 4.58, yield the appropriate activation energy of solution in units of kilocalories per mole.

The hypothesis that the slope of the solubility line for the base element of an alloy is the same as the slope of the solubility line for the pure element (i.e., the second assumption) can be tested by analysis of covariance (ref. 18). The results of a comparison of the slopes of the regression lines are as follows. For the HS-25 alloy slope compared to the elemental cobalt slope, the 95-percent confidence interval for the difference between slopes is $0.51\pm2.53\times10^3$. For the SICROMO-9M alloy slope compared to the elemental iron slope, the 95-percent confidence interval for the difference between slopes is

$0.98\pm1.86\times10^3$. Since the interval in both cases includes zero, the hypothesis cannot be rejected.

For the reasons just discussed, the activation energy of solution for the cobalt- and iron-base alloys was taken to be

$$Q_S^{HS-25} \approx Q_S^{H-8187} \approx Q_S^{Co} = 16.4 \text{ kcal/mole } (68.5\times10^3 \text{ J/mole})$$

$$Q_S^{9M} \approx Q_S^{AM-350} \approx Q_S^{Fe} = 11.0 \text{ kcal/mole } (46.0\times10^3 \text{ J/mole})$$

No data are available for solution rate activation energy in mercury. This activation energy is probably related to the energy needed by the dissolving species to diffuse through an impurity or reaction-product barrier film at the solid-liquid interface. In the tests reported herein, there was no deliberate addition of a mercury solution rate inhibitor (e. g., zirconium or titanium, which tend to form nitride surface films (ref. 19)). Further, X-ray observations showed good wetting of surfaces in contact with mercury, which suggests the absence of an oxide or oil impurity film at the solid-mercury interface. It was therefore assumed that Q_{sr}^A is zero.

Listed in table VIII are the ΔH_i values for material-transport steps S_1, S_2, S_3, and S_4 calculated from equations (20) to (23) and the appropriate Q^A values.

Variation of penetration as function of y. - Where the concentration of dissolved material is also a function of y (i.e., rate control by S_2, S_3, or S_4), a variation of corrosion penetration down the capsule wall may be expected. Corrosion penetration should decrease in a regular manner (determined by the solution rate constants and convective diffusion parameters) from $y = 0$ where $c(y) = 0$ to $y = -l$ where $c(y) \lesssim c_o$.

Mechanism changes. - The proposed corrosion model for selective attack implicitly presupposes a change of mechanism during the progress of corrosion. Phenomenologically, this can be viewed as a consequence of changes wrought in the length and nature of the material-transport path. Analytically, this is made evident when the kinetic relation for the overall corrosion reaction (i.e., for all steps of the model viewed together) is examined. The overall kinetic relation for the selective attack model is

$$\alpha t = \gamma_1 p^2 + \gamma_2 p + \gamma_3 p^2 + \gamma_4 p \tag{24}$$

where γ_1, γ_2, γ_3, and γ_4 are constants related to the respective constants of the transport steps, as described in the section Time-law constant, and p is the corrosion penetration predicted by the selective attack model. (See appendix B for derivative of eq. (24).) It is seen from equation (24) that when p is small either S_2 or S_4 (depending on the relative values of γ_2 and γ_4) must be the rate-determining step. Depending

on the relative values of the constants, either S_1 or S_3 will become rate controlling as corrosion penetration increases with time. To recapitulate, the selective attack model predicts that the initial rate-controlling step follows a linear corrosion rate (associated with a boundary-region process). Further, during the progress of corrosion, this initial rate-controlling step is succeeded eventually by a step that follows a parabolic corrosion rate (associated with a diffusion process).

No material-transport path change is postulated for the uniform attack model. Therefore, where the uniform attack model applies, no mechanism change may be expected.

DISCUSSION OF RESULTS

Corrosion Rates and Rate-Controlling Steps

Inferences of the rate and the rate-controlling step in the corrosion attack of mercury on the materials tested are presented herein. These inferences are based primarily on a comparison of the experimental and theoretical kinetic constants that are derived in the ANALYSIS section and listed in tables VII and VIII, respectively. Subsidiary evidence as to the nature of the rate-controlling step is found in a comparison of the observed and predicted variation of corrosion penetration along the capsule wall. The universally observed wedge-like penetration pattern in longitudinal sections of corroded capsules corresponds to the predicted variation of corrosion penetration when any step but S_1 is rate controlling.

Cobalt-base alloys, HS-25 and H-8187. - In the initially observed corrosion regime, data group 1, the corrosion rate was parabolic, and the probable rate-controlling step was S_3. In the succeeding corrosion regime, data group 2, the corrosion rate was linear. In the case of both alloys, the ΔH_r values fell between the ΔH_i values for S_2 and S_4. Because of the relatively small difference between ΔH_i for S_2 and S_4, the uncertainty in the estimate of ΔH_r, and the assumption made in estimating the ΔH_i values, an unequivocal choice of rate-controlling step cannot be made.

Iron-base alloy, SICROMO-9M. - In the initially observed corrosion regime, data group 1, the corrosion rate was linear. The probable rate-controlling step was taken to be S_4. The judgment was somewhat arbitrary because, although the ΔH_r value was closer to ΔH_4 than to ΔH_2, it was significantly larger than ΔH_4. (See the discussion for AM-350.) In the succeeding corrosion regime, data group 2, the corrosion rate was parabolic, and the probable rate-controlling step was S_3.

Iron-base alloy, AM-350. - Over the entire test range, the corrosion rate was linear. The probable rate-controlling step was S_4. Again, as in the case of SICROMO-9M,

this judgment is somewhat arbitrary. The result for AM-350 and SICROMO-9M ($\Delta H_r > \Delta H_4$ by 8 to 12 kcal/mole (3×10^4 to 5×10^4 J/mole)) is similar to that reported by Horsley (ref. 4) for the corrosion of mild steel in mercury from 900° to 1200° F (755° to 922° K), assuming boundary-layer control. From Horsley's calculations ΔH_r was greater than ΔH_4 by 11 kilocalories per mole (4.6×10^4 J/mole). These discrepancies between experimental and theoretical activation energy may possibly reflect inaccuracy in the iron solubility data or, conversely, an incorrect corrosion model.

Mechanism Change and Corrosion Regimes

Analysis of the experimental data indicates that mechanism changes occur during the progress of corrosion for all alloys studied, with the exception of AM-350. Theoretical consideration of the corrosion models support these results.

When a change in mechanism takes place, the corrosion reaction enters a new corrosion regime. Three corrosion regimes can be characterized from this present study: linear I, parabolic, and linear II. In the following exposition of the corrosion regimes, figure 12 is used as a graphic example. In this figure are the 1100° F (866° K) corrosion
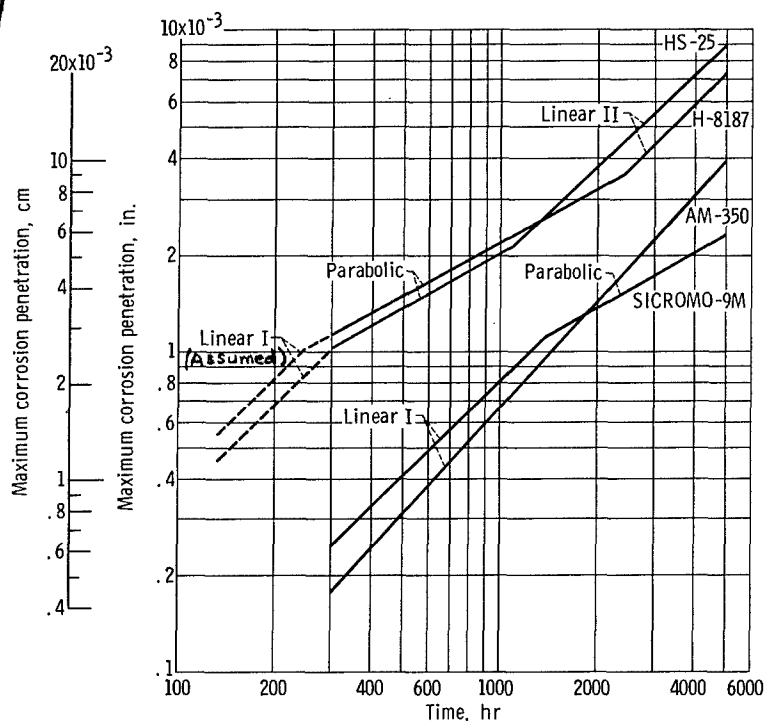

Figure 12. – Corrosion rate of test alloys at 1100° F (866° K).

rate curves, derived from equation (7), and the pertinent values found in table VI for HS-25, H-8187, SICROMO-9M, and AM-350. The solid portion of each curve covers the test range. The dashed portions are conjectural.

Linear I. - At the start of each test and for some time thereafter the inner surface of a capsule is relatively smooth, with no deep corrosion penetrations. As such, the corrosion reaction is best represented by the uniform attack model. Accordingly, the initial corrosion rate is expected to be linear for all materials.

A linear rate is maintained when the capsule wall exhibits a continuous uniform recession. Such behavior is exemplified by the AM-350 alloy, as indicated in figure 5. Attack on the AM-350 alloy progresses by grain-boundary penetration. Since, however, the groove angle formed is approximately 130°, the corrosion attack moving on a wide-angle front results effectively in wall recession.

Parabolic. - Continuing corrosion attack on the materials tested, other than AM-350, results in the formation of a channel-penetrated or porous-network type of corrosion zone. This developing corrosion zone interposes itself as a new link in the mass-transport chain. Transport of matter across the channeled or porous region occurs by diffusion along the quiescent liquid paths created by mercury contained within the channels or the network. When the corrosion channels or network reach a sufficient depth, the rate of material transport along the liquid diffusional path becomes slower than along other paths in the transport chain. Thus, the rate-controlling step changes, and the initially observed linear corrosion rate becomes parabolic. The change of rate from linear to parabolic is continuous since the physical changes occurring in the corrosion zone are continuous and progressive. For simplicity of presentation, no attempt was made to indicate a continuous change in rate on the pertinent curves in figure 12.

The formation of channels in the SICROMO-9M alloy can be attributed to intergranular attack advancing with a small groove angle, approximately 50°. No satisfactory explanation can be offered for the pronounced difference in magnitude of the groove angles produced in the SICROMO-9M and AM-350 alloys, which in the case of the latter alloy leads to wall recession.

The formation of a porous Co_3W and Co_2W network in the HS-25 and H-8187 alloys can be attributed to leaching of the more soluble elements from the corrosion zone. Since Co_3W and Co_2W are not found in the as-received material nor in the material outside the corrosion zone of the tested capsules, it can be concluded that these compounds are formed in situ by reaction of the residual elements following the leaching process.

Figure 12 indicates that at 1100° F (866° K) SICROMO-9M exhibits a linear corrosion rate until about 1400 hours, after which the rate becomes parabolic. A comparable linear-to-parabolic rate change for HS-25 and H-8187 remains unconfirmed because of the lack of sufficient short-time data. The initial linear rate curve shown for these alloys in figure 12 is conjectural.

Linear II. - In the case of the HS-25 and H-8187 alloys, a change in density probably occurs within the corrosion zone as a result of leaching. From mass balance considerations (see table IV), it can be estimated that the density of the fully developed HS-25 and H-8187 corrosion zones is, respectively, 0.24 and 0.18 the density of the original material. The density changes and the accompanying volume changes probably induce stresses within the corrosion-zone network and between the network and the base material. When the stresses exceed the critical shear stress, cracks develop (see fig. 3, p. 10). The cracks allow the flowing mercury direct access to the base material. As a result, the diffusional path through the porous corrosion zone is bypassed, and the corrosion rate reverts from parabolic to linear. The cracks, once initiated, can be expected to grow as corrosion continues and to be accompanied by spalling; thus, the linear corrosion rate is maintained. This particular corrosion behavior is closely analogous to certain oxidation reactions where parabolic-to-linear rate changes occur when developed stresses cause cracking and scaling of oxide layers.

In figure 12, the corrosion rate of HS-25 and H-8187 at 1100° F (866° K) changes from parabolic to linear at 1100 and 2400 hours, respectively. This change is consistent with the first appearance of cracks in the corrosion zone of test capsules. Cracks appear between 1000 and 2000 hours for HS-25 and between 2000 and 5000 hours for H-8187.

Liquid Flow Velocity

Liquid flow velocity cannot be treated as an independent variable in reflux capsule corrosion tests. In these tests the mercury film velocity is a function of the vaporization rate, which in turn is a function of temperature. Since, however, the temperature-velocity functional relation is relatively weak and the temperature range of investigation is relatively narrow, the effect of velocity on the test results was assumed to be negligible. This was justified as follows: The data from the linear rate group for each material were fitted by multiple regression analysis to the estimating equation

$$\log p_r = a_r + b_r \log t + \frac{B_r}{T} - 0.75 \log T \tag{25}$$

The estimating equation was derived from equation (19) with the appropriate substitution for the constants D_l, c_o, and h in terms of T (see appendix C). Equation (25) reflects the effect of velocity on corrosion with the assumption of S_4 control. The residual error variance and the coefficients b_r and B_r (eq. (25)) did not differ significantly from the values found in table VI for the pertinent data fit to equation (7).

Although velocity effects were not discernible in this investigation, such effects

should be manifest at high liquid flow velocity. Speculations and observations on the effect of high flow velocity on erosion and corrosion are presented in the following paragraphs.

Erosion. - Flow velocities within the reflux capsules were 0.2 to 0.4 inch per second (0.5 to 1.0 cm/sec), too low to incur erosional effects. However, at higher velocity, materials inclined to intergranular penetration are likely to suffer erosion through grain removal. Further, as a consequence of this erosion, the mode of corrosion attack will differ from that observed in the capsules. In the case of SICROMO-9M, for example, initial intergranular attack would produce a layer of peripherally corroded grains at the alloy-liquid interface. Through the action of a high stream velocity these grains would be readily swept away. As a consequence of continuing erosional grain removal, channel formation would be curtailed. With channel formation curtailed, mechanism change is precluded, and corrosion attack would continue in the linear I regime.

This speculation is supported by the results of SICROMO-9M forced-convection-boiling mercury loop tests run at liquid flow velocities as great as 108 inches per second (274 cm/sec) (refs. 20 and 21). No channeled-corrosion zone was found, although intergranular attack was evident. Also, the wall thickness loss was considerably greater than that predicted by the capsule tests for comparable time and temperature conditions.

Corrosion. - The effect of liquid flow velocity on corrosion is related to the nature of the rate-controlling step of the corrosion reaction. When boundary-layer diffusion S_4 is rate controlling, corrosion will be proportional to v^n, where n is 1/3 for laminar flow and n is 1/2 to 1 for turbulent flow. When solution S_2 is rate controlling, equation (12) indicates that penetration is proportional to $c_o - c(y)$. The term $c(y)$ is dependent on solution rate and stream velocity (as defined by the convective diffusion parameters of the stream) and can range in value from 0 to c_o. Consequently, p_2 will vary from a maximum when $c(y) = 0$ to 0 when $c(y) = c_o$. For two cases of interest, p_2 is independent of v: for reflux capsules at the point of maximum penetration (i.e., $y = 0$, $c(y) = 0$) and for high flow, low solubility rate situations (i.e., $c(y) = $ constant).

The results of this investigation suggest that, for AM-350 and SICROMO-9M alloys, S_4 control is likely in the linear corrosion regimes; no resolution could be reached on the question of S_2 or S_4 control for the HS-25 and H-8187 alloys. Evidence supporting S_4 control is found in the results of tests of forced-convection corrosion loops fabricated of SICROMO-9M alloy (refs. 20 and 21) and HS-25 alloy (unpublished results of tests by A. Vary of Lewis). In all these tests, mercury saturation temperature was about 1100° F (866° K). The velocity range covered was from 12 to 108 inches per second (30.5 to 274 cm/sec). Although the penetration data as a function of velocity exhibit a large variability, in all cases corrosion penetration is greater than that expected for linear corrosion rates with S_2 control.

SUMMARY OF RESULTS

A total of 108 mercury reflux capsule tests were performed on the cobalt-base alloys HS-25 and H-8187 and the iron-base alloys SICROMO-9M, AM-350, and AM-355. (The latter two alloys are treated as one alloy.) The test temperature range was 1000° to 1300° F (811° to 977° K), and test times were as long as 5000 hours.

Metallographic analysis revealed that corrosion resulted in either uniform attack, characterized by wall recession (AM-350), or selective attack, characterized by a leached-out porous corrosion zone (HS-25 and H-8187) or a channel-like grain-boundary-penetrated corrosion zone (SICROMO-9M).

Values of the experimental kinetic constants (i.e., the time-law constant b_r and the activation energy ΔH_r) were obtained from a multiple regression fit of the corrosion data to the estimating equation

$$\log p_r = a_r + b_r \log t + \frac{\Delta H_r}{2.303\ RT}$$

where p_r is the observed corrosion penetration, t is test time, T is test temperature, R is the gas constant, and a_r is a constant.

The theoretical kinetic constants b_i and ΔH_i, for each of i steps of proposed corrosion models, were obtained from transport theory relations and the pertinent boundary conditions.

Analysis of the experimental data indicated that mechanism changes occurred during the progress of corrosion for all alloys studied, with the exception of AM-350. Theoretical consideration of the corrosion models supported these results.

Inferences of rate and rate-controlling step were made by comparing ΔH_i and b_i for each step in the proposed corrosion model with ΔH_r and b_r, respectively. Because of the lack of data needed to estimate the activation energy for several pertinent processes, there is some uncertainty in the estimated ΔH_i values. Consequently, the inference of rate-controlling step must be considered as tentative.

Two corrosion regimes were inferred from the HS-25 and H-8187 alloy data. The first was a parabolic rate regime with liquid diffusion as the probable rate-controlling step. This regime was succeeded by a linear rate regime with boundary-layer diffusion as the probable rate-controlling step. Although not experimentally verified, there is good reason to believe that the parabolic regime is preceded by a linear rate regime.

Two corrosion regimes were inferred from the SICROMO-9M alloy data. The first was a linear rate regime with boundary-layer diffusion as the probable rate-controlling

step. This regime was succeeded by a parabolic rate regime with liquid diffusion as the probable rate-determining step.

A single corrosion regime of linear rate with boundary-layer diffusion as the probable rate-controlling step was inferred in the case of the AM-350 alloy.

Lewis Research Center,
National Aeronautics and Space Administration,
Cleveland, Ohio, October 24, 1967,
120-27-02-18-22.

APPENDIX A

MERCURY VAPORIZATION RATE AND CONDENSATE FILM PROPERTIES

A determination was made of the temperature profile along the capsule and the heat loss from the top of the capsule at several temperature levels in order to estimate the mercury vaporization rate in the reflux capsule tests. A typical capsule was used with five thermocouples spot welded to the wall in the positions shown in figure 13. Other
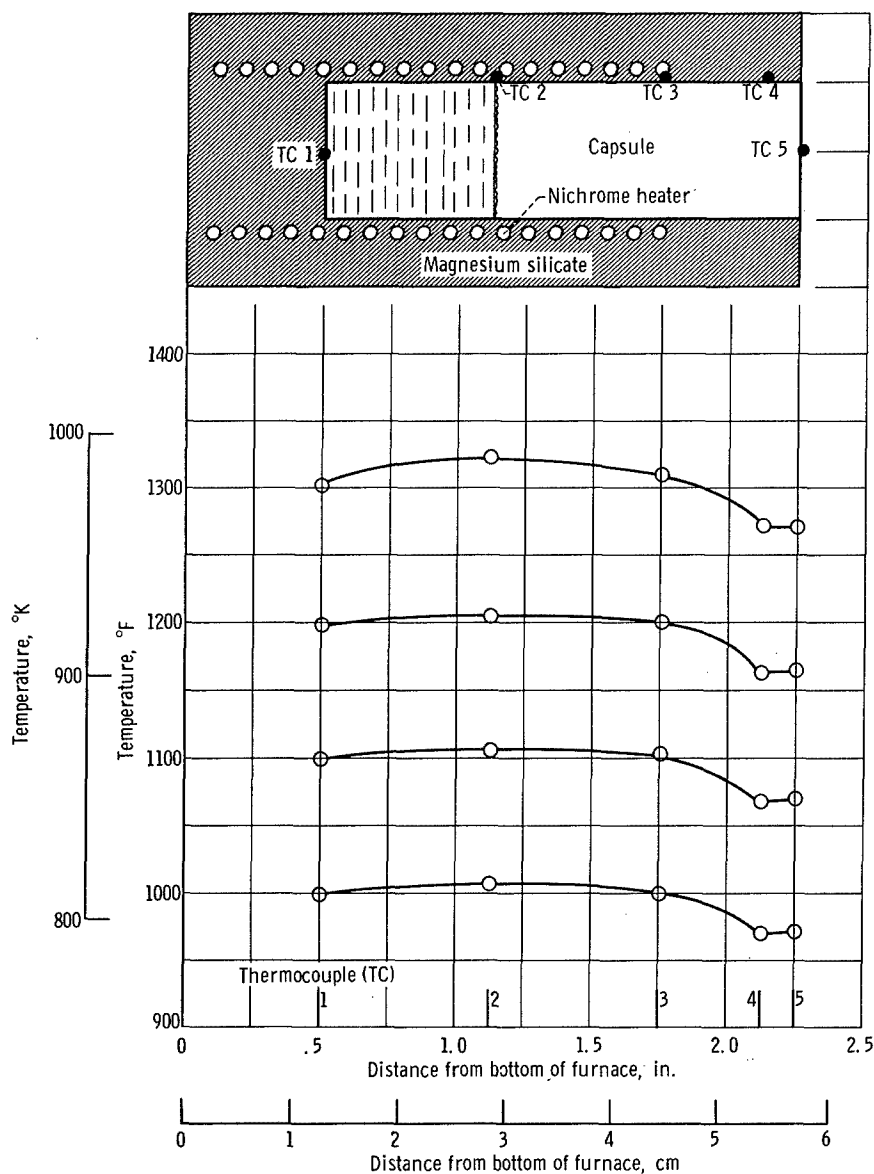

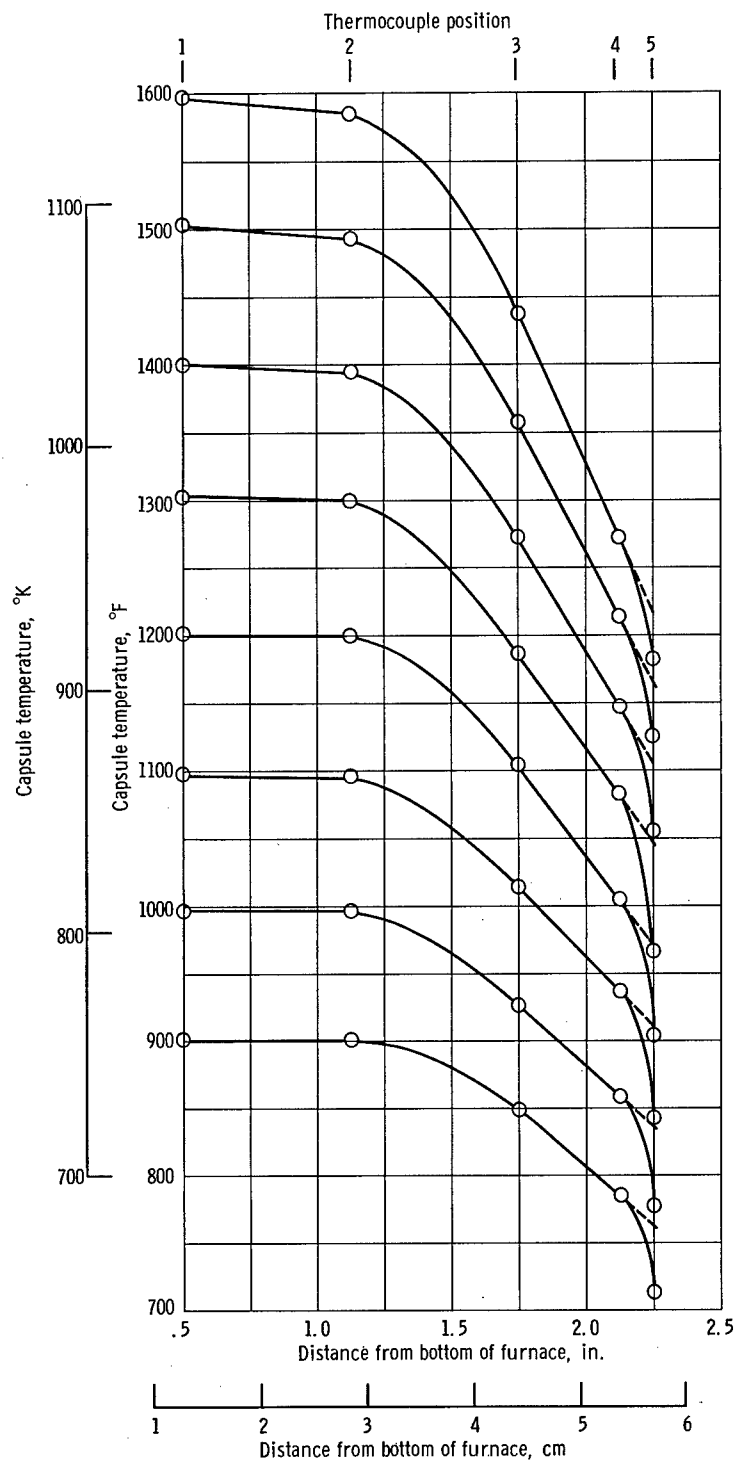Figure 13. – Typical temperature profiles for a capsule containing mercury.

Figure 14. - Typical temperature profiles obtained with an empty capsule.

thermocouples were distributed throughout the capsule furnace assembly. The setup was operated at 1000°, 1100°, 1200°, and 1300° F (811°, 866°, 922°, and 977° K) with the capsule one-third filled with mercury. The capsule was then removed, emptied of mercury, and resealed in vacuum with an electron-beam welder. The capsule was re-installed in the furnace and operated over a range of temperature from 900° to 1600° F (755° to 1144° K).

The temperature profiles for the runs made with mercury in the capsule are shown in figure 13. The slight temperature rise indicated along the lower two-thirds of the capsule is probably a result of the proximity of thermocouples 2 and 3 to the heater. The temperature drop observed over the top one-third of the capsule is most likely somewhat larger than the true drop, because of heat-conduction loss from convective cooling of the thermocouple wire.

Temperature profiles obtained with the evacuated empty capsule are shown in figure 14. The profiles show a nearly uniform temperature for the lower portion of the capsule and a temperature drop of 200° to 400° F (111° to 222° K) for the upper portion of the capsule. The anomalous temperature drop indicated by the top thermocouple (5) probably results from two factors. The first factor is an added resistance to heat conduction at the thermocouple location produced by the dimple machined in the surface of the capsule. The wall thickness at the dimple was 0.010 to 0.020 inch (0.025 to 0.051 cm) as compared with 0.040 inch (0.10 cm) for the nominal wall thickness. The second factor is an enhanced heat-conduction loss down the thermocouple wires caused by convective cooling. It is assumed that the true top temperature is that value obtained by straight-line extrapolation of the temperatures given by thermocouples 3 and 4.

The heat loss from the top of the capsule was calculated from the following equation:

$$q = \kappa A \frac{\Delta T}{L} \tag{A1}$$

where κ is the thermal conductivity, A is the cross-sectional area of the capsule wall, and $\Delta T/L$ is the slope of the linear portion of the temperature-profile curve between the thermocouples 3 and 5 of figure 14. Heat loss from the capsule top is plotted in figure 15 as a function of true top-surface temperature of the empty capsule.

Since the heat loss from the top of the capsule for any given top temperature is independent of whether the capsule is filled or empty, values of heat loss for the filled capsule tests can be obtained directly from figure 15.
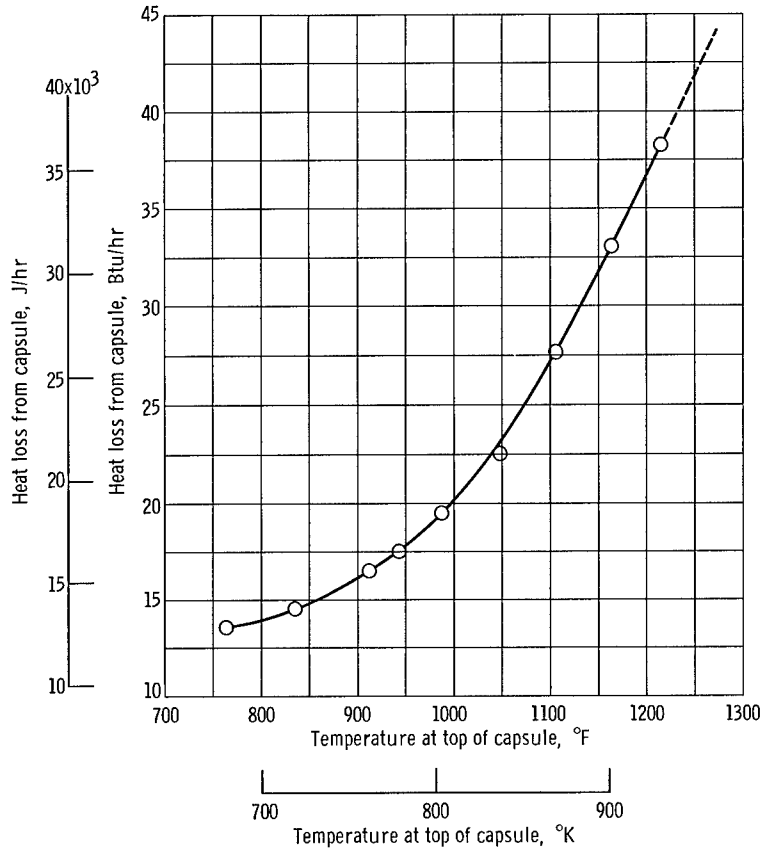
Figure 15. - Heat loss from capsule top as function of temperature.

The vaporization rate m was obtained from the relation

$$m = \frac{q}{H_v \rho} \qquad (A2)$$

where H_v is the latent heat of vaporization and ρ is the density of mercury. Calculated values of m are given in table V for capsule bottom temperatures of 1000°, 1100°, 1200°, and 1300° F (811°, 866°, 922°, and 977° K).

Average velocity $\bar{v}$ over the film cross section is (ref. 11, p. 671)

$$\bar{v} = \frac{gh^2}{3\nu} \qquad (A3)$$

where h is the film thickness, ν is the kinematic viscosity, and g is the gravitational

43

constant. A relation for the film thickness can be obtained as follows. The average velocity is equal to the vaporization rate m divided by the flow cross-sectional area of the film. Since h ≪ d, where d is the capsule inside diameter, the flow cross-sectional area is approximately equal to πdh. Substituting m/πdh for $\bar{v}$ in equation (A3) and solving for h yield

$$h = \left(\frac{3m\nu}{\pi dg}\right)^{1/3} \tag{A4}$$

The calculated film thickness and average velocity are given in table V for capsule temperatures of 1000°, 1100°, 1200°, and 1300° F (811°, 866°, 922°, and 977° K).

APPENDIX B

DERIVATION OF KINETIC RELATION FOR SELECTIVE ATTACK MODEL

The kinetic relation for the selective attack model can be obtained by considering the overall corrosion reaction in terms of a flux of matter j which has to overcome a series of resistances r_i. Each resistance is associated with a corresponding step S_i. The sum total of all the steps compose the mass-transfer path. The driving force for each step is a concentration difference Δc_i. Thus, analogous to current flow in an electric series circuit,

$$j = \frac{\sum \Delta c_i}{\sum r_i} \tag{B1}$$

When parallel paths exist, as for example in the case of volume and grain-boundary diffusional paths $S_{1,1}$ and $S_{1,2}$ in the solid diffusion step S_1 (fig. 8), the total resistance r_1 is given by the expression

$$\frac{1}{r_1} = \frac{1}{r_{1,1}} + \frac{1}{r_{1,2}}$$

Consequently, when $r_{1,1} \approx r_{1,2}$, $r_1 \approx r_{1,2}/2$ or when $r_{1,1} > r_{1,2}$, $r_1 \approx r_{1,2}$. Thus, the total resistance may be expressed in terms of the smaller of the parallel path resistances.

Two types of resistances may be considered: (1) resistance $r_{i,b}$ associated with steps involving a boundary region (e. g., S_2 and S_4) and (2) resistance $r_{i,d}$ associated with steps involving diffusional processes (e. g., S_1 and S_3). The relation between $r_{i,d}$ and the depth of corrosion penetration p is

$$r_{i,d} = \gamma_i p \tag{B2}$$

where γ_i is a characteristic constant for the ith step. Resistance $r_{i,b}$ may be expressed simply as

$$r_{i,b} = \gamma_i \tag{B3}$$

When the flux of matter is constant,

$$j = \varphi \frac{dp}{dt} \tag{B4}$$

where φ is a proportionality constant. Combining equations (B1) and (B4) and making the appropriate substitution for the r_i terms yield the following corrosion-rate expression for the selective attack model:

$$\varphi \frac{dp}{dt} = \frac{\sum\limits_{i=1}^{4} \Delta c_i}{\gamma_1 p + \gamma_2 + \gamma_3 p + \gamma_4} \tag{B5}$$

If it is assumed that Δc_i is constant, integrating equation (B5) and combining constants into a new constant α (the integration constant being 0 since $p = 0$ at $t = 0$) yield the following kinetic relation:

$$\alpha t = \gamma_1 p^2 + \gamma_2 p + \gamma_3 p^2 + \gamma_4 p \tag{B6}$$

APPENDIX C

ACTIVATION-ENERGY CALCULATIONS

The following equation was used to calculate the activation energies for each material-transport step:

$$\Delta H_i = \frac{R \, d(\ln k_i)}{d \frac{1}{T}} \tag{4}$$

Listed below are the pertinent expressions for k_i obtained from equations (9), (12), (15), and (19) and evaluated at the point of maximum attack. An appropriate proportionality constant ϵ_i is included:

$$k_1 = \epsilon_1 D_s^{1/2} \tag{C1}$$

$$k_2 = \epsilon_2 k_{sr} c_o \tag{C2}$$

$$k_3 = \epsilon_3 (D_\ell c_o)^{1/2} \tag{C3}$$

$$k_4 = \epsilon_4 \frac{D_\ell c_o}{h} \tag{C4}$$

Diffusion in Solid S_1

$$\Delta H_1 = \frac{R \, d\left(\ln \epsilon_1 D_s^{1/2}\right)}{d \frac{1}{T}} \tag{C5}$$

The temperature dependence of D_s is as follows:

$$D_s = D_o \exp\left(\frac{-Q_d^A}{RT}\right) \tag{C6}$$

where D_o is a constant and Q_d^A is the effective activation energy for diffusivity in alloy A. Substituting for D_s in equation (C5) and performing the differential operation yield

$$-\Delta H_1 = 0.5\, Q_d^A \tag{C7}$$

Solution S_2

$$\Delta H_2 = \frac{R\, d\left(\ln\, \epsilon_2 k_{sr} c_o\right)}{d\,\dfrac{1}{T}} \tag{C8}$$

The temperature dependence of k_{sr} and c_o is given by the following relations:

$$k_{sr} = \lambda\, \exp\left(\frac{-Q_{sr}^A}{RT}\right) \tag{C9}$$

$$c_o = \lambda'\, \exp\left(\frac{-Q_s^A}{RT}\right) \tag{C10}$$

where λ and λ' are constants and Q_s^A and Q_{sr}^A are, respectively, the effective activation energy of the solution and the solution rate in mercury of the elements of alloy A. Substituting for k_{sr} and c_o in equation (C8) and performing the differential operation give

$$-\Delta H_2 = Q_s^A + Q_{sr}^A \tag{C11}$$

Diffusion in Static Liquid S_3

$$\Delta H_3 = \frac{R\, d\, \ln\left[\epsilon_3 (D_\ell c_o)^{1/2}\right]}{d\,\dfrac{1}{T}} \tag{C12}$$

The temperature dependence of D_ℓ can be approximated by the Stokes-Einstein relation:

$$D_l = \frac{k_b T}{6\pi r_o \eta_o} \exp\left(\frac{-Q_v}{RT}\right) \tag{C13}$$

where k_b is the Boltzmann constant, η_o is a constant, r_o is the radius of the diffusing substance (approximately the same for all metal atoms considered in this study), and Q_v is the activation energy for viscous flow. Combining equations (C12), (C10), and (C13) and differentiating yield

$$-\Delta H_3 = 0.5\left(Q_s^A + Q_v + RT\right) \tag{C14}$$

Convective Diffusion S_4

$$\Delta H_4 = \frac{R\, d\left(\ln \epsilon_4 \dfrac{D_l c_o}{h}\right)}{d\dfrac{1}{T}} \tag{C15}$$

An analysis of the mercury vaporization data (table V) indicates that h is proportional to $T^{1.75}$. Substituting the appropriate temperature-dependent relations for D_l, c_o, and h into equation (C15) and differentiating give

$$-\Delta H_4 = Q_s^A + Q_v + 2.75\,RT \tag{C16}$$

APPENDIX D

SYMBOLS

A cross-sectional area of capsule wall, m^2

a constant

B_r regression coefficient

b time-law constant

c concentration, kg/m^3

c_o equilibrium solubility concentration, kg/m^3

D_l diffusion coefficient in liquid, m^2/hr

D_s diffusion coefficient in solid, m^2/hr

d capsule inside diameter, m

f constant

G solution mass flux, $kg/(m^2)(hr)$

g gravitational constant, $(N\text{-}m^2)/kg^2$

H_v latent heat of vaporization, J/kg

ΔH activation energy, $J/mole$

h condensate film thickness, m

j mass flux, $kg/(m^2)(hr)$

k specific rate constant

k_b Boltzmann constant, $J/^oK$

k_{sr} solution rate constant, m/hr

L linear portion of temperature profile, m

l vertical length of condensate film, m

m vaporization rate, m^3/hr

n constant

p corrosion penetration or wall recession, m

Q_d^A effective activation energy for chemical diffusivity in alloy A, $J/mole$

Q_s^A effective activation energy for solution of elements of alloy A, $J/mole$

Q_{sr}^A effective activation energy for solution rate of elements of alloy A, $J/mole$

Q_v activation energy for viscous flow, $J/mole$

q heat loss, J/hr

R gas constant, $J/(^oK)(mole)$

R_m^2 coefficient of multiple determination

r mass flux resistance, hr/m

r_o radius of diffusing species

S material-transport step

s standard deviation

s^2 variance

T absolute temperature, ^oK

t time, hr

v liquid flow velocity, m/hr

$\bar{v}$ average film flow velocity, m/hr

w mass transport, kg

$\alpha, \beta, \gamma,$
$\epsilon, \eta_0, \lambda$ } constants

κ thermal conductivity,
       $J/(m)(hr)(^{\circ}K)$

ν kinematic viscosity, m^2/hr

ξ convective diffusion parameter

ρ density, kg/m^3

Subscripts:

b   bulk; boundary-region process

d   diffusional process

i   transport step

k   transport step parallel path

r   derived from corrosion data

s   rate-controlling transport
       step

w   wall

REFERENCES

1. Rosenblum, L.: Liquid Metals for Aerospace Electric-Power Systems. J. Metals, vol. 15, no. 9, Sept. 1963, pp. 637-641.

2. Slone, Henry O.: SNAP-8 Development Status. Space Power Systems Advanced Technology Conference. NASA SP-131, 1966, pp. 147-168.

3. Epstein, Leo F.: Static and Dynamic Corrosion and Mass Transfer in Liquid Metal Systems. Chem. Eng. Prog. Symp. Ser., vol. 53, no. 20, 1957, pp. 67-81.

4. Horsley, G. W.: Mass-Transport and Corrosion of Iron-Based Alloys on Liquid Metals. J. Nucl. Energy, Pt. B: Beactor Tech., vol. 1, no. 2, 1959, pp. 84-91.

5. Lyons, Richard N., ed.: Liquid-Metals Handbook. Second ed. Rep. No. NAVEXOS P-733 (Rev.), U.S. AEC and Dept. of the Navy, Bureau of Ships, June 1952, pp. 164-169.

6. Kubaschewski, O.; and Hopkins, B. E.: Oxidation of Metals and Alloys. Second ed., Butterworth, Inc., 1962, pp. 70-142.

7. Ezekiel, Mordecai; and Fox, Karl A.: Methods of Correlation and Regression Analysis. Third ed., John Wiley & Sons, Inc., 1959.

8. Harrison, J. D.; and Wagner, C.: The Attack of Solid Alloys by Liquid Metals and Salt Melts. Acta Met., vol. 7, no. 11, Nov. 1959, pp. 722-735.

9. Crank, J.: The Mathematics of Diffusion. Clarendon Press (Oxford), 1956, pp. 111-120.

10. Levich, Veniamin G. (Scripta Technica, Inc., trans.): Physicochemical Hydrodynamics. Prentice-Hall, Inc., 1962, p. 693.

11. Jakob, Max: Heat Transfer. Vol. 1. John Wiley & Sons, Inc., 1949, pp. 451-464.

12. Yang, Ling; and Derge, G.: General Considerations of Diffusion in Melts of Metallurgical Interest. Physical Chemistry of Process Metallurgy - 1. Vol. 7 of the AIME Met. Soc. Conferences. Interscience Publ., 1961, pp. 503-521.

13. Smithells, Colin J.: Metals Reference Book. Vol. 2. Third ed., Butterworth, Inc., 1962.

14. Parkman, M. F.; and Whaley, D. K.: The Solubility of Iron, Chromium, Nickel, Cobalt, and Vanadium in Mercury and Concentrations of Those Elements Found in Mercury After Contact with Iron-, Cobalt-, and Vanadium-Base Alloys. Rep. AN-957 (NASA CR-53939), Aerojet-General Nucleonics, July 1963.

15. Weeks, J. R.: The Solubility of Chromium, Cobalt, and Iron in Mercury. Paper presented at 20th Annual National Association of Corrosion Engineers, Chicago, Mar. 9-13, 1964.

16. Jangg, G.; and Palman, H.: Die Loeslichkeit verschiedener Metalle in Quecksilber. Zeit fuer Metallkde., vol. 54, no. 6, June 1963, pp. 364-369.

17. Marshall, A. L.; Epstein, L. F.; and Norton, F. J.: The Solubility of Iron in Mercury at 25-700°. J. Am. Chem. Soc., vol. 72, no. 8, Aug 1950, pp 3514-3516.

18. Duncan, Acheson J.: Quality Control and Industrial Statistics. Rev. ed., Richard D. Irwin, Inc., 1959, pp. 717-723.

19. Kammerer, O. F.; Weeks, J. R.; Sadofsky, J.; Miller, W. E.; and Gurinsky, D. H.: Zirconium and Titanium Inhibit Corrosion and Mass Transfer of Steels by Liquid Heavy Metals. Trans. AIME, vol. 212, no. 1, Feb. 1958, pp. 20-25.

20. Kimura, L. A.: Corrosion Mechanism Loop-1 Summary Report. Rep. No. AN-SNAP 67-346, Aerojet-General-NEMO, Jan. 25, 1967.

21. Anon.: SNAP-8 Materials Report for July - December 1966. Rep. No. 3349 (NASA CR-72257), Aerojet-General Corp., Jan. 1967.